Engineering of poly(glycerol sebacate) scaffolds

by

Kamal Asadipakdel

Submitted to the Graduate School of Engineering and Natural Sciences
in partial fulfilment of the requirements for the degree of
Master of Science

Sabanci University

July 2022

Engineering of poly(glycerol sebacate) scaffolds

Kamal Asadipakdel

Material Engineering and Science, MSc. Thesis, 2022
Thesis Supervisor: Asst. Prof. Sibel Çetinel
Thesis Coadvisor: Assoc. Prof. Mustafa Kemal Bayazıt

ABSTRACT

40% of blindness in humankind is because of a problem in the human cornea. The only effective cure for most human cornea diseases is transplantation which is costly, and 1 out of 3 is unsuccessful due to rejection. Tissue engineering is an emerging field that can be a promising solution for human cornea disease. Fabricating a suitable scaffold for cell proliferation and attachment is where engineering can step in to carry a burden in this field. For human cornea, the scaffold should be transparent to provide proper eyesight, and transparent polymer can be a good option as a scaffold for human cornea tissue engineering. Transparent polymers are widely used in various applications, such as tissue engineering, optoelectronics, automotive, biosensors, etc. Most well-known transparent polymers are not biodegradable, among which poly (glycerol sebacate) PGS has shown promising properties in bio applications. However, there is minimal knowledge about PGS's optical properties and crosslinking mechanism. In this study, three PGS pre-polymer with different molecular weight is synthesized, shaped into 300-micron films, and each pre-polymer is crosslinked at different durations. The sample with the highest molecular

weight, PGS3, exhibits a decrease in transmittance from 86 % to 78% in UV-vis data. XPS, FTIR, UV-vis spectroscopy, and Refractometer were utilized to shed light on the correlations between crosslinking and optical properties. This research suggests that the pre-PGS chains with acid endings react with secondary OH in other PGS chains to establish a link between the chains during crosslinking. By doing so, the binding energy of carbon electrons energy decreases, and they get excited by electromagnetic waves with lower energies. Carbon 1 s electrons in ester function in PGS3 decrease from 289.16 eV to 288.6 eV, causing PGS color formation in samples with a higher degree of crosslinking. The Refractive index of crosslinked PGS does not indicate a significant change. The refractive index of PGS3 increased by 1.488 and 1.491 when the crosslinking time escalated from 1 hour to 48 hours. PGS1-PGS3 films, crosslinked for 48 hours, seeded with human corneal epithelium and retinal pigment epithelial (ARPE-19) cells to investigate the effect of cell culture on the PGS films' optical properties.

Keywords: PGS; Tissue Engineering; Human cornea; Synthesis and characterization; Scaffolds

Poli(gliserol sebakat) iskelelerinin mühendisliği

Kamal Asadipakdel

Malzeme Mühendisliği ve Bilimi, Msc. Tez, 2022

Tez Danışmanı: Dr.Öğr.Üyesi Sibel Çetinel

Tez Danışmanı: Doç.Dr. Mustafa Kemal Bayazıt

Özet

İnsanoğlundaki körlüğün %40'ı insan korneasındaki bir sorundan kaynaklanmaktadır. İnsan kornea hastalıklarının çoğu için tek etkili tedavi, maliyetli olan transplantasyondur ve 3'te 1'i reddedilme nedeniyle başarısız olur. Doku mühendisliği, insan kornea hastalığı için umut verici bir çözüm olabilecek, gelişmekte olan bir alandır. Hücre çoğalması ve bağlanması için uygun bir yapı iskelesi üretmek, mühendisliğin bu alanda bir yük taşımak için devreye girebileceği yerdir. İnsan korneası için, uygun görüş sağlamak için iskele şeffaf olmalıdır ve şeffaf polimerler insan kornea doku mühendisliği için bir iskele olarak iyi bir seçenek olabilir. İyi bilinen şeffaf polimerlerin çoğu biyolojik olarak parçalanamaz olmasına rağmen, poli (gliserol sebakat) PGS, biyolojik uygulamalarda umut verici özellikler göstermiştir. Ancak, PGS'nin optik özellikleri ve çapraz bağlama mekanizması hakkında sınırlı bilgi bulunmaktadır. Bu çalışmada, farklı moleküler ağırlığa sahip üç PGS ön polimeri sentezlenmiş, 300 mikron kalınlığında filmlere şekillendirilmiş ve her bir ön polimer farklı sürelerde çapraz bağlanmıştır. En yüksek moleküler ağırlığa sahip numune olan PGS3, çapraz bağlama süresi 1 saatten 48 saate yükseldiğinde görünür ışığın geçirgenliğinde %86'dan %78'e bir azalma sergiler. Çapraz bağlama ve optik özellikler arasındaki korelasyonlara ışık tutmak için XPS, FTIR, UV-vis spektroskopisi ve Refraktometre kullanılmıştır. Bu araştırma, asit uçlu ön-PGS zincirlerinin, çapraz

bağlama sırasında zincirler arasında bir bağlantı kurmak için diğer PGS zincirlerinde ikincil OH ile reaksiyona girdiğini göstermektedir. Böylece karbon elektronlarının bağlanma enerjisi azalır ve daha düşük enerjili elektromanyetik dalgalar tarafından etkilenmiş. PGS3'teki ester fonksiyonundaki karbon 1s elektronları 289.16 eV'den 288.6 eV'ye düşerek, daha yüksek derecede çapraz bağlamaya sahip numunelerde PGS renk oluşumuna neden olur. Çapraz bağlı PGS'nin refraktiv indeksi önemli bir değişiklik göstermez. Çapraz bağlama süresi 1 saatten 48 saate yükseldiğinde PGS3'ün kırılma indeksi 1.488 ve 1.491 arttı. 48 saat boyunca çapraz bağlanmış, insan kornea epiteli ve retina pigment epiteli (ARPE-19) hücreleri ile tohumlanmış PGS1-PGS3 filmleri, hücre büyümesi ve çoğalması için biyouyumlu bir yapı iskelesi sağladı. Memeli hücre kültürünün PGS filmlerinin optik özelliklerini değiştirmediği bulundu.

Anahtar Kelimeler: PGS; Doku mühendisliği; İnsan korneası; Sentez ve karakterizasyon; İskeleler.

AKNOWLEDGMENTS

First, I am really grateful to have chance to work under supervision of my thesis advisor, Dr. Sibel Çetinel. Owning to possessing an integrous personality, I have always considered her as a family member rather than an academic collaborator. Without exaggeration, our world needs this type of people more than ever, and I have been so lucky to take full advantage of her emotional and motivational support.

I am also thankful to my fully respected co-advisor, Dr. Mustafa Kemal bayazit, a symptom of perseverance and delegation. Thanks to his guiding and invaluable comments, I could improve my productivity to the highest possible extent.

I would like to thank my fellow friends Sevilay Burcu Şahin, Ebru demir, Hande Eda Şutova, for their priceless help, whom I had the chance to know and collaborate with during the last two years of my academic life. They helped me to overcome all the difficulties and burdens on my way in completing this thesis.

Special thanks to my friends Mohammad Jafarpour, Ali Toufani, Ali Ansari Hamedani, Vahid charkhesht, Amin Abdollahzadeh, Shayan Ramazanzadeh, Roozbeh Saghatchi, and Hadi Abbaszadeh, Seyedali seyed sarraf who have supported me along the way during my study at Sabanci University.

The last but not the least, I would like to express my everlasting grace to my best friend, my love and my wife, Saba Hajizadeh, and my parents for supporting and encouraging me throughout my years of study and my life in general. This accomplishment would not have been possible without them.

This work is funded by 2232 International Fellowship for Outstanding Researchers Program of TUBITAK (Grant number 118C371). The funder had no role in study design, data collection or analysis, the decision to publish, or the preparation of this thesis.

Table of Contents

Table of Figures

Table of Tables

1. CHAPTER 1: INTRODUCTION

1.1 Background

Tissue engineering has shown great potential in utilizing the coalescence of cells, engineering, and materials to rehabilitate, preserve, enhance, and substitute various human body tissues. One of the main areas of tissue engineering is synthesizing, designing, and fabricating scaffolds for tissue regenerations. Scaffolds are porous solid biological materials with three dimensions that are meant to accomplish one or more of the following tasks: (i) enhance the interactions between cell and material, cell attachment, and extracellular matrix deposition; (ii) guarantee the differentiation, viability, proliferation of cells by allowing the adequate exchange of oxygen, carbon dioxide, nourishment, and regulatory elements; (iii) biodegrade at a managed speed that resembles tissue renewal and (iv) indicates insignificant inflammation or poisonous in vivo [1].

1.2 Polymers in medical science

Polymers under the term “biopolymers” have been used widely in bio applications [2]. Both synthetic and natural polymers are utilized in tissue engineering, drug delivery, and implants. The famous synthetic biopolymers are polyesters, polyamides, Teflon, poly (β-amino esters), polyethylene, polyanhydrides, poly (amido amines), Silicones, and poly (ortho esters), polyacrylates [3]. Some of these polymers are suitable for soft tissue regeneration, such as Poly(Glycerol Sebacate), silicones, polyurethanes, and polyethylene [4].

According to the aim of this research to replace a transparent tissue (human cornea), some polymers are transparent but not a good candidate for tissue engineering due to their lack of biocompatibility and biodegradability [3]. Some of their polymers are such as Acrylic

(polymethylmethacrylate), Teflon AF (amorphous fluoropolymer), Lexan (polycarbonate), Butyrate (cellulose acetate butyrate), and PETG (glycol-modified polyethylene terephthalate) [5–7]. Among the aforementioned polymers, Poly(Glycerol Sebacate) is a good candidate for human cornea tissue engineering [8]. In the following, a short literature review about it is available.

1.3 Synthesis, characterization, and fabrication of Poly(Glycerol Sebacate)

PGS, a biocompatible and biodegradable synthetic polymer, was introduced in 2002 by Y. Wang et al. by reaction of glycerol with sebacic acid. PGS has 1 MPa fracture strength at 270 % tensile stress and 17 ± 6% weight loss due to degradation in PBS solution after 60 days [9,10].

1.3.1 Synthesis of PGS

Synthesis of PGS has two main stages; one, synthesis of pre-PGS, and second the crosslinking of pre-polymer to obtain rigid yellowish solid [11]. The synthesis of pre-PGS can be demarcated into three main approaches (see Fig. 1):

- Polycondensation under the vacuum by conventional heat [9,10]
- Synthesis by enzyme [12,13] and
- Polycondensation by microwave [10,14]

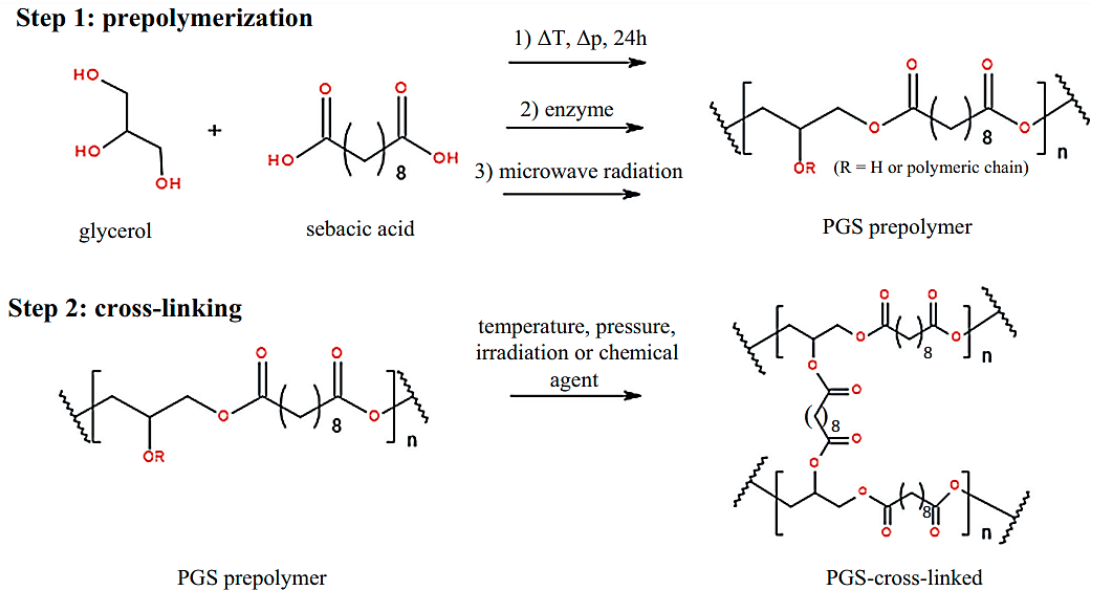

Figure 1 synthesis approaches of PGS

The most popular method is the first one, glycerol reacts with sebacic acid at 120 °C under a vacuum, with a 1:1 ratio for 24 hours. A silicone oil bath provides heat as a conventional method. The pressure for this method is 40 mtorr under argon atmosphere. Later, the pre-PGS is crosslinked at 40 mtorr pressure and 120 °C for 48 h [9,15–18].

For enzymatic synthesis, Candida antarctica lipase B (CALB) is utilized. CALB is widely used in industry and academia due to its wide application in esterification, hydrolysis, and amidation. It has a higher tendency to react with primary OH than secondary ones. The synthesis process is mixing equimolar (5 mmol of each) glycerol and sebacic acid alongside 200 mg of CALB at 60 °C under gentle stirring for 34 hours. After removing the solvent and washing with acetone, the produced polymer is colorless to yellowish gel according to its molecular weight [12].

The energy of the reaction can be provided by microwave radiation. The synthesis time can decrease by microwave in comparison to the conventional method. The most efficient radiation

application happens when the interval is included in the process—for example, 60 sec 600 W redaction with 10-sec intervals [10,19,20].

1.3.2 Properties of PSG

recognizing the properties of any material top to bottom is essential to clarifying its actual capacity for potential applications. PGS has been exposed to various examinations to acquire a more profound comprehension of its properties. The accompanying areas cover these parts of the improvement of PGS:

Mechanical properties of PGS

Three criteria govern the mechanical properties of PGS (i) monomer's molar ratio, (ii) crosslinking temperature, and (iii) crosslinking time [9,10,21,22]. Chen et al. indicated that the young modulus of PGS changed from 0.056 MPa to 0.22 MPa, and 1.2 MPa by increasing the crosslinking temperature from 110 °C to 120 °C and 130 °C, respectively [22,23]. In another study, J. M. Kemppainen revealed that by adding to the molar ratio of sebacic acid, the tangent modulus of PGS is increasing. The polymers with molar ratios of (glycerol to sebacic acid) 4:3, 1:1, and 3:4 indicated tangent modulus of 0.2, 1.5, and 2.5 MPa, respectively [21].

The PGS stress-strain curve reveals the elastomeric behaviors of PGS [9]. The elastomeric behavior originates from the PGS's covalent bond, 3d network, and hydrogen bonds[23]. The ultimate tensile strength of PGS is 0.5 to 1.5 MPa at 100% to 300% strain [10,21,24].

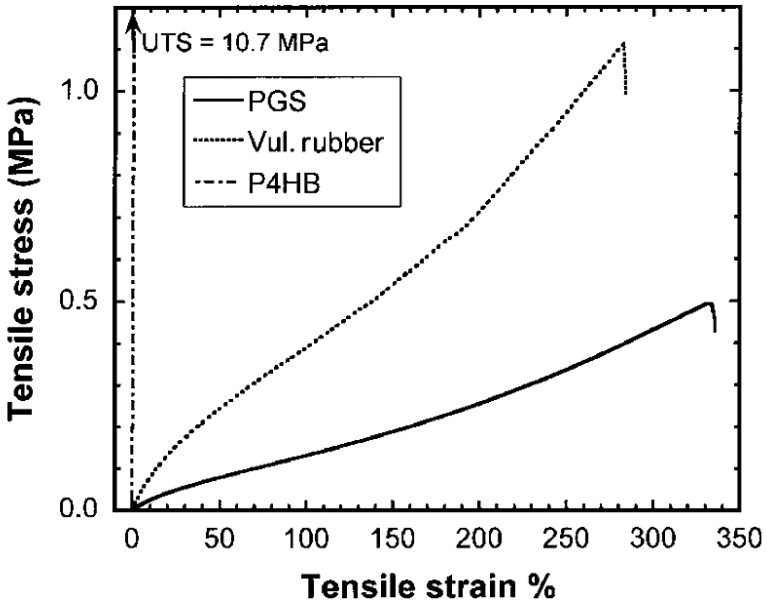

Figure 2 Tensile Stress-strain curve of PGS. vulcanized rubber, and P4HB [9]

Physio-chemical properties of PGS

PGS is almost colorless with a fully transparent polyester. Fig. 1 shows the structure of PGS with the presence of secondary OH as a preferred site for branching and crosslinking. Wang et al. have conducted the Fourier-transform infrared spectroscopy (FTIR) analysis of PGS. There is a sharp peak at 1730 cm^{-1} corresponding to the C=O peak, a broad peak in the range of 3000 to 3400 cm^{-1} related to the OH group, and 1640 cm^{-1} related to stretching of the C-O bond, and 2930 cm^{-1} and 2855 cm^{-1} attributed to C-H bonds. As the degree of esterification increases, the intensity of the OH peak is reduced [10,25]. Also, the structure of PGS has been analyzed by Nuclear Magnetic Resonance (NMR) spectroscopy by Jaafer et al., confirming the OH group's attach to the polymer's backbone Fig. 3a the OH chemical shift at 5.3 ppm (red circle). The OH is a polar function causing the hydrophilicity of the PGS [10,25,26].

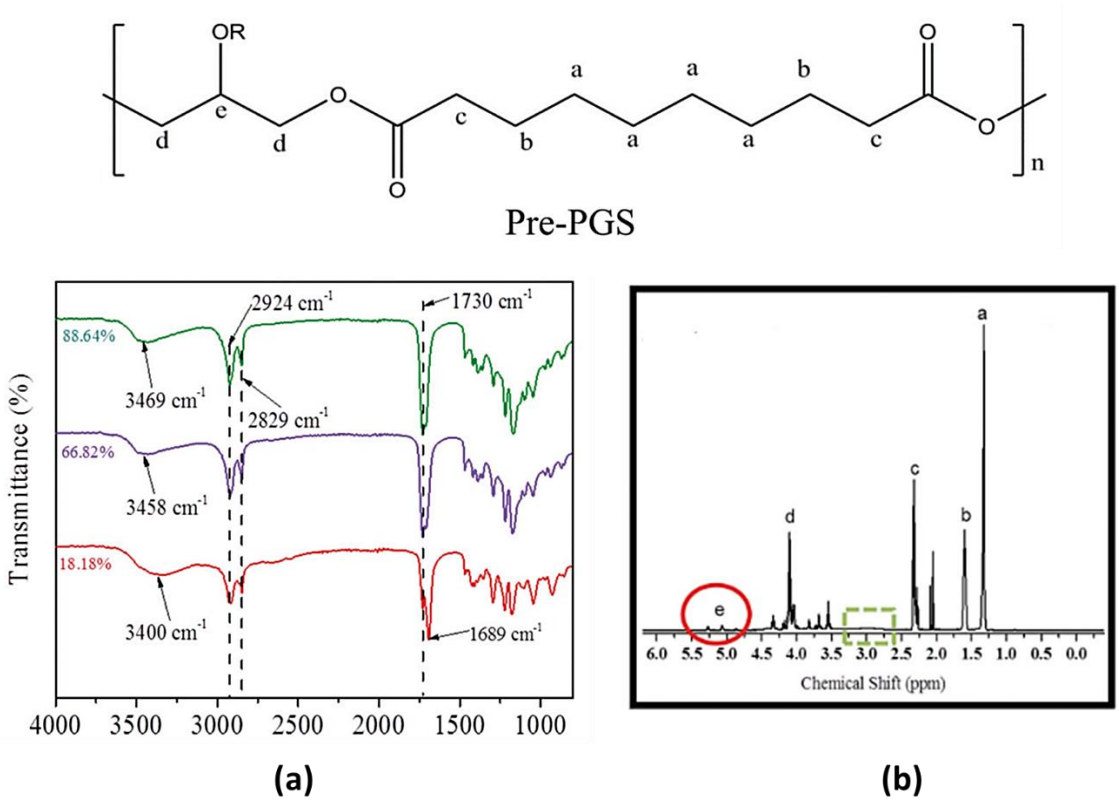

Figure 3 (a) FTIR analysis of PGS with various degrees of esterification and (b) NMR analysis of PGS and its corresponding hydrogen groups [10]

Thermal properties and Crystallinity of PGS

PGS is a thermoset semicrystalline polymer. In DSC curve prepared by Jaafer et al. presented in Fig. 4 indicates Tg, crystallization, and melting peaks. Pre-PGS has crystallization and melting peaks. However, as crosslinking continues, the polymer chains have less mobility to rearrange themselves to crystallize. Thus, the peaks are getting smaller. On the other hand, the Tg peak is almost fixed at -25 °C in pre-PGS and crosslinked samples. The pre-polymer indicates a melting peak at 10.2 °C and a crystallization peak at -18.3 °C. Polymer is fully amorphous after 37 °C.

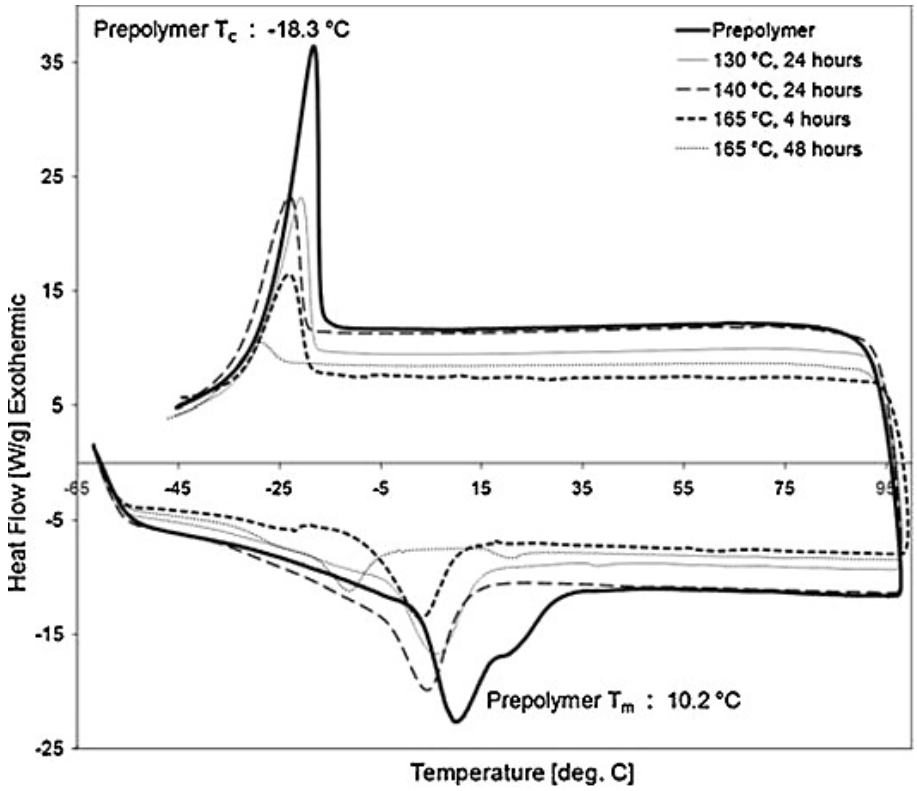

Figure 4 DSC analysis of pre-PGS and samples that cured at different durations

Biocompatibility of degradation behavior of PGS

Plenty of research studied the degradation behavior of PGS due to its significant effect on potential applications, specifically biomedical applications. The degradation of polymers is usually a progressive process that alters its physicochemical properties over time [9,17,24]. PGS degradation starts from the surface and decomposes to its monomers in the presence of water due to hydrolysis [9,13,27]. Glycerol is alcohol abundant in the human body, and the FDA approved its biocompatibility. Also, sebacic acid is available in the human body as a metabolic intermediate; however, its high concentration is toxic to the cells [9]. Accordingly, the polymer should be tuned so that PGS degradation and subsequent secretion of sebacic acid must happen gradually [19].

In another study, 10-mm discs of PGS with different crosslinking durations were prepared and implanted for various durations. In the early stages of implanting, the is only on the surface (Fig. 5a), and as time proceeds, the degradation progress deeper [24].

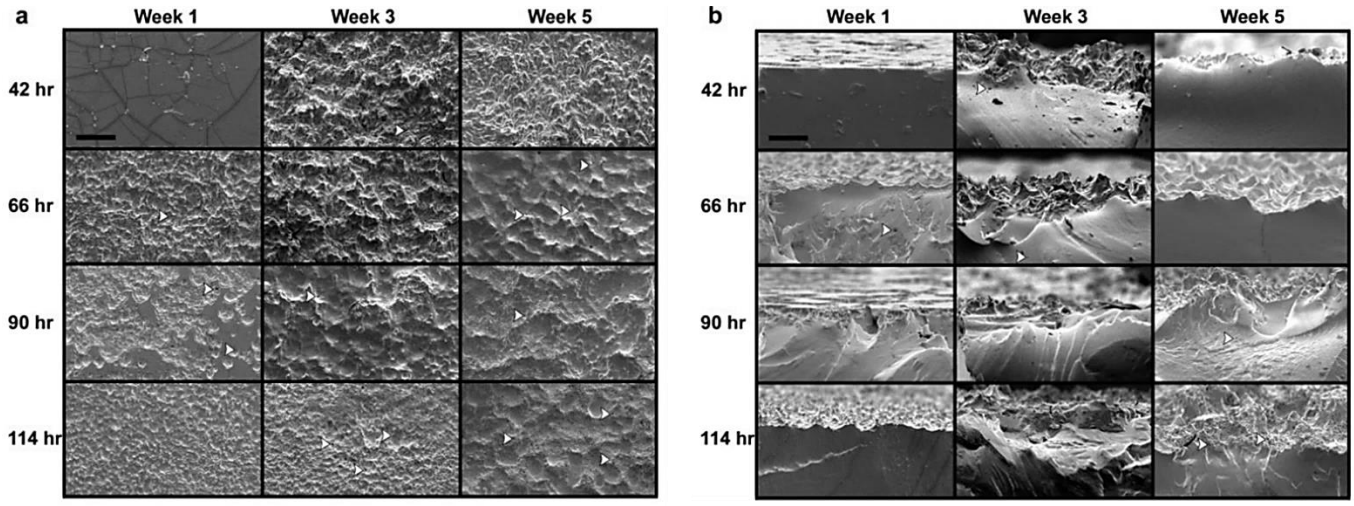

Figure 5 Scanning electron microscopy (SEM) images of PGS implants crosslinked for 42, 66, 90, and 114 h, implanted for 1, 3, and 5 weeks. The degradation in (a) surface and (b) cross-section is apparent [24].

The fundamental mechanism of degradation is the cleavage of the ester functions. In contrast to mass degradation, for which the mechanical strength diminishes well ahead of mass loss, the changing the shape and volume of PGS, going through surface degradation, there is a slow loss of tensile strength, comparative with mass loss (per unit initial region) happens. As the mass loss changes directly with time, noticeable enlarging and better geometry maintenance are noticed (see Fig. 6) [9,25,28,29].

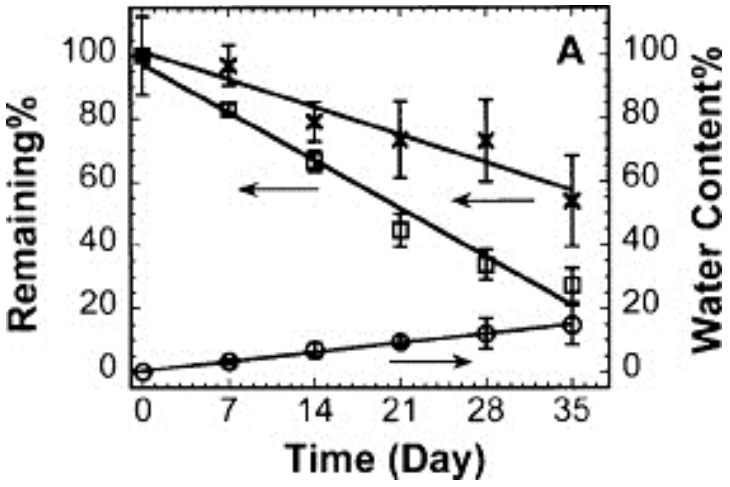

Figure 6 degradation behavior of PGS samples implanted in Sprague-Dawley rats from day 1 to 35 days. Changes in mass (□); mechanical strength (×); water content (○) [28].

In vitro and in vivo tests have shown that PGS is a proper candidate for soft tissue regeneration applications [30]. In vivo tests in rats revealed that the implants have a minor inflammation. Compared to PGLA, PGS shows the same behavior; only there is little evidence of fibrous capsule formation [24,30].

1.3.3 Fabrication techniques for PGS-based biomaterials

Pre-PGS has demonstrated to be promptly processable utilizing different methods. The most straightforward is to give it a reasonable shape involving in-mol polymerization joined with crosslinking. However, notwithstanding the objective shape, a few variables should be considered while planning the material for potential tissue designing applications: these incorporate porosity, mechanical properties, and biocompatibility. While examining PGS handling, one ought to note that the pre-polymer structure is mostly handled (in non-crosslinked structure). Probably the most ordinarily involved methods for poly(glycerol sebacate) handling are depicted in the following.

Solvent casting

This method is the most widely used approach to fabricating biomaterials based on PGS. It consists of three steps: 1) dissolving the polymer in a solvent (pre-PGS); 2) placing the solution into a provided mold or vessel (i.e., Petri dish); and 3) evaporating the solvent and crosslinking the product [19].

For PGS and PGS-based materials, dimethylformamide (DMF), tetrahydrofuran (THF), and dimethyl carbonate (DMC) are the most commonly used solvents [31]. The particulate leaching technique often supports the solvent casting method. This treatment aims to obtain larger pores optimal for cell growth and development. Thus, solid particles are brought into the polymer arrangement and cleaned out of the material after the crosslinking [19]. Lee et al. utilized 25-32-μm grounded salts, which after the development of the last component, were cleaned out in a water shower or solid particles [32]. The polymers produced by this method are often exposed to freeze-drying to remove the solvents while maintaining the structure.

Thermally-induced phase separation

The thermally induced phase separation (TIPS) strategy depends on enlisting stage division in the liquid-liquid or solid-liquid systems. The standard PGS fabricating process utilizing this technique can be partitioned into 4 phases: 1) the pre-polymer dissolving, 2) freezing of the solution, 3) freeze-drying, and 4) crosslinking of the polymer. The product is highly porous, like foam (see Fig. 7) [19]. In a study, the porous scaffold of PGS by this method is prepared with an inorganic filler (Hexamethylene diisocyanate (HDI)) has been produced by Martin Frydrych and Biqiong Chen [33].

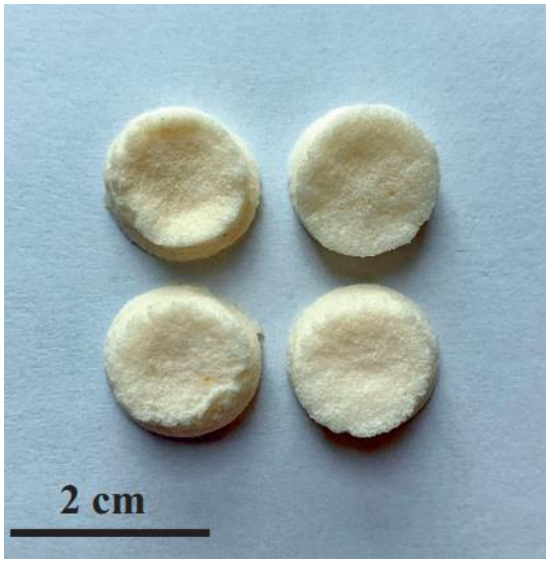

Figure 7 Porous membrane of PGS with inorganic filler obtained by TIPS method [19]

Electrospinning

Electrospinning is a process in which a polymeric solution with a polar solvent is stretched by electrostatic force from a higher voltage to a lower voltage to form random nanofibers. Electrospun fibers' diameter can be from a couple of microns to 10 to 50 nanometers. For some studies, to align the fibers, the collector should be a turning drum, and the speed of the drum determines the degree of the unidirectionality of fibers [34–38].

When it comes to PGS, electrospinning has two main barriers that make it impossible to be spun. First, the low molecular weight of PGS, and Second the thermoset characteristics of PGS. Thermoset polymers should be crosslinked to have desirable mechanical and thermal properties; on the other hand, crosslinked polymers cannot be shaped, dissolved, or melted. One option can be shaping the pre-PGS, but they will melt down during crosslinking at 130 °C, much higher than the melting temperature of pre-PGS (37 °C) [19].

Two options are suggested to overcome these barriers: first, use another polymer such as PLA as a carrier [39]. Second, utilize PGS as a component in other polymers such as poly(lactic acid)

(PLA), polycaprolactone (PCL), or poly(methyl methacrylate) (PMMA) [40,41]. Fig. 8 indicates the procedure F. Flaig et al. suggested for preparing the PGS/PLA blend [40].

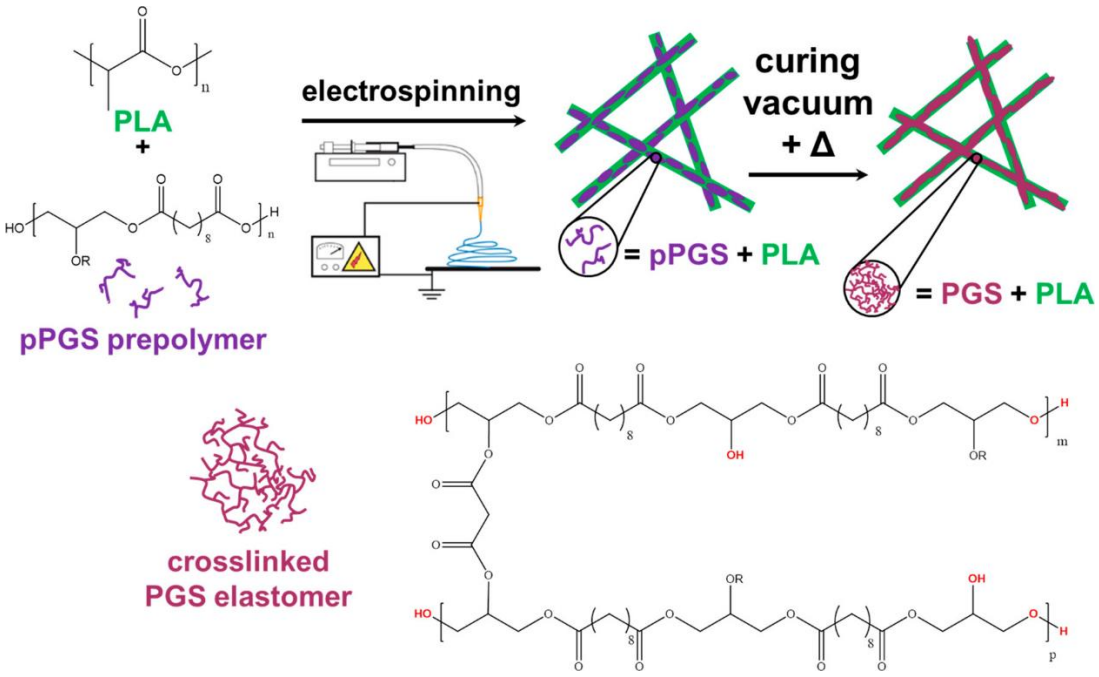

Figure 8 is the graphical presentation of the preparation of the electrospun blend of PGS/PLA [40].

3D printing methods

3D printing is a versatile technique in which, with the assistance of a computer, 3D models can be fabricated. The same problems for electrospinning are also valid for 3D printing. In the literature, some research has embedded acrylate function in the structure of PGS to obtain PGSA, which can be crosslinked after printing by UV radiation [11,14,42–44].

1.4 Biomedical application of PGS

As discussed, PGS's remarkable properties make it a good candidate for soft tissue Eng. applications such as cardiovascular, retina, cartilage, and nerve tissues. Additionally, PGS has been utilized for tissue adhesives and drug delivery applications [43].

1.4.1 Tissue engineering applications

PGS is progressively being utilized to foster membranes or scaffolds as cell conveyance vehicles in various tissue engineering (TE) methodologies. The prepared scaffolds should be biocompatible, give an excellent surface to the cells to stick, and have the option to direct and coordinate the cells. Additionally, scaffolds should uphold cell development, by which cells ought to be kept up within an applicable state by compelling dispersion of supplements and the arrival of waste. When new tissue is shaped, the scaffolds should degrade in a controlled way, and the debasement items should be non-poisonous and very much endured in the body [43,45,46].

Cardiac TE

Cardiovascular diseases (CVDs) are the top-ranked disease-causing of death worldwide, and this data signifies the importance of finding fruitful cures [43]. Most diseases are only cured by transplantation, which has problems such as high cost, rejection of tissue, and scarcity of heart donors [22,40]. PGS has introduced itself with great potential as scaffolds for myocardial tissue Eng. Most studies are around using PGS for cardiac patches. [22,40,47]. These heart patches aim to provide healthy cardiac cells for the infarct region and convey left ventricular limit, i.e., mechanical support to the left ventricle. The main challenge in fabricating these patches is the mechanical math of the scaffolds with the native myocardium. Some studies have investigated tailoring PGS mechanical properties to match the cardiac tissue by changing the crosslinking conditions (time and temperature) [23,40,43]. Fig. 9 indicates the approach for fabricating the cardiac patches [48].

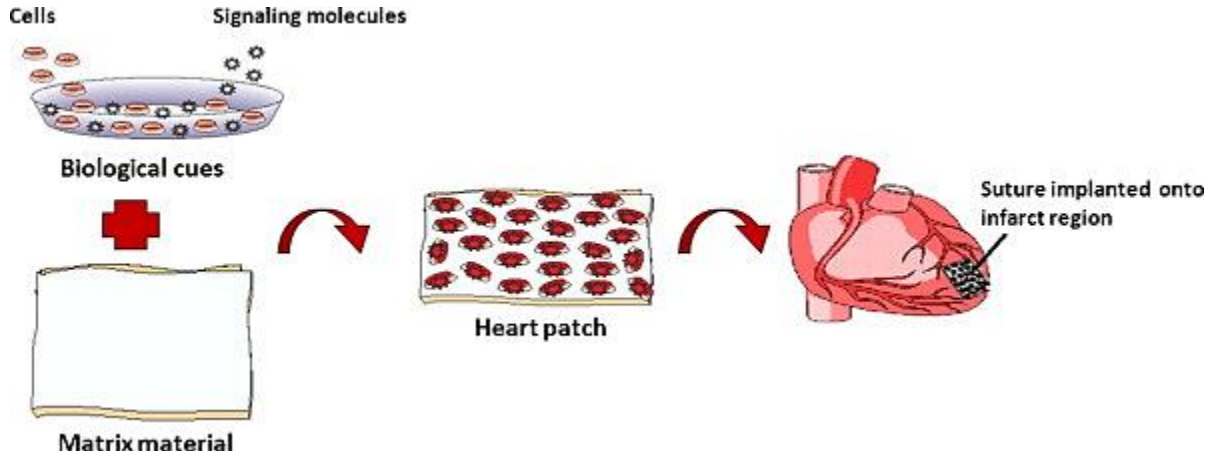

Figure 9 the suggested approach by KL Christman et al. for fabricating the cardiac patches [48]

Nerve TE

The best treatment for nerve tissue engineering is autografting, which raised some problems like donor site mortality, lack of donor tissues, and insufficient functional recovery [30]. To tackle these problems, natural and synthetic biomaterials have been investigated. Synthetic biomaterials such as Artificial materials such as poly(organo)phosphazenes, poly(glycolide) (PGA), poly(lactide-ε-caprolactone), poly(l-Lactide) (PLLA), poly(Dl-lactide-co-glycolide) (PLGA), biodegradable polyurethanes, and trimethylene carbonate–caprolactone copolymers are suggested as a conduit for neural cells guidance. All of these polymers have shown inflammatory and swelling side effects. [49–51]. A.Sundbacka et al. researched PGS as a guide for nerve tissues [52]. In this research, they have chosen the PLGA as a control. Several in vivo and ex vivo experiments using primary Schwann cells have been conducted. PGS indicated similar to superior results compared to PLGA. PGS has shown significantly fewer inflammatory side effects and minor swelling in comparison to PLGA [52]. Fig. 10 indicates the photomicrographs of PGS and PLGA cultured on them.

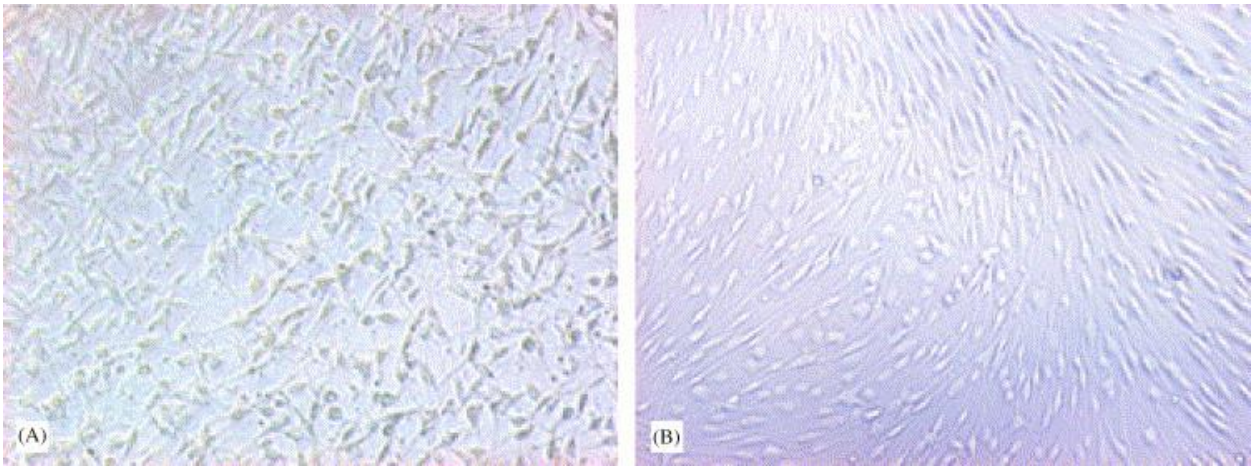

Figure 10 photomicrographs (100x) of PGS and PLGA cultured by primary Schwann cells [52].

Retinal TE

The retina is a backer tissue of the human eye that transduces the light to an electrical charge subsequently used by neurons to make the visual data. Currently, there is no feasible cure for retina degeneration. Transplantation can be an option; however, the donation problems are also valid for this process. Additionally, the proper perseverance of the organization and structure of the retina should be assured to reach valid phototransduction to the host neurons [53,54]. The technique for proper organization of retinas is using immature RPCs (see Fig.11). Laster by differentiation and growing cells will choose their preferred direction. In this context, PGS has been developed as short-term structural support for cell growth and differentiation [55–57].

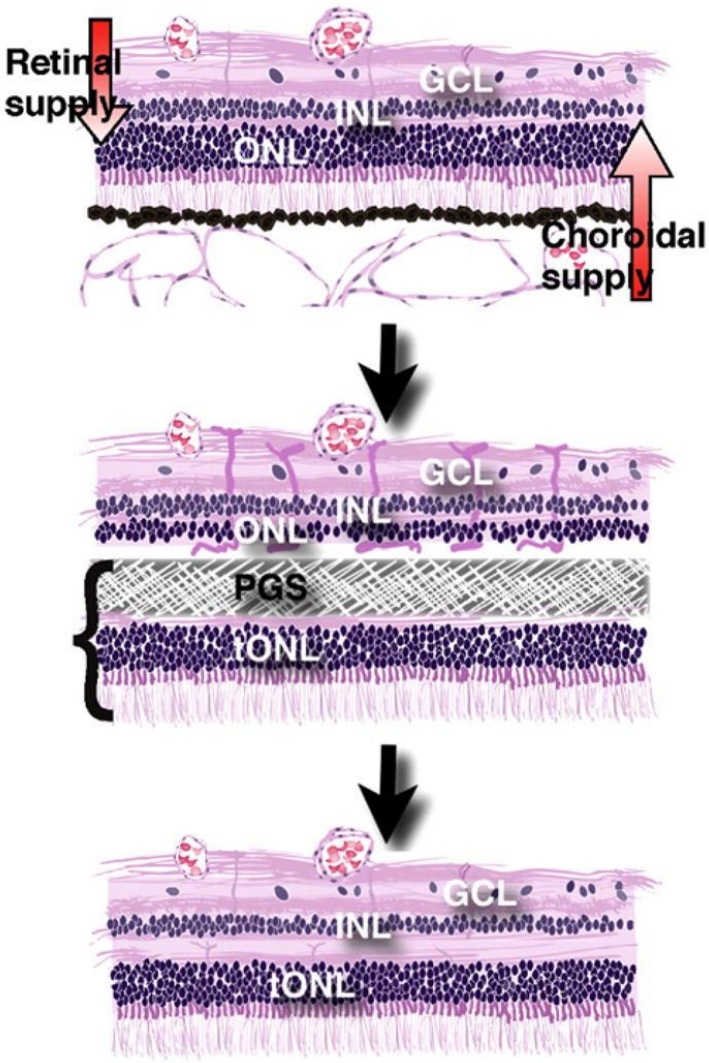

Figure 11 Outline of the composite retinal join model. Top: The in vivo retina. The choroid supplies the photoreceptors in the external atomic layer (ONL). In contrast, the retinal vessels supply the inward retinal cells in the inward atomic and ganglion cell layer (INL and GCL). Center: When the composite join, comprising of photoreceptors in a transfer external atomic layer (tONL) melded with a PGS film, is put in the subretinal space, the layer impedes the nutritional help to the host ONL, which prompts ischemia and eliminates have photoreceptors. Base: Following PGS layer debasement, the leftover internal retina of the host coordinates with the relocated photoreceptors (tONL), making another retina with all [57]

Cornea TE

Salehi et al. have prepared PGS/PCL electrospun nanofibers with different ratios to obtain the best nanofiber morphology. The obtained fibers are fully aligned, and their average diameter is 300-

500 nm. They have suggested these fibers as a good candidate for human eye stroma mimicking ECM [8]. Another study investigated the mechanical properties of the fabricated membrane [58].

1.4.2 Drug delivery

The objective of controlled delivery is to move a proper measure of medications to the impacted region of the patient's body without causing unfavorable secondary effects on different issues. One of the most well-known applications for drug conveyance frameworks is in the broad referenced field of wound recuperating. Notwithstanding, they are additionally progressively being utilized to battle malignant growth and treat different sicknesses like periodontal or visual diseases, including diabetic retinopathy [59,60].

PGS implants have been developed for anticancer drug delivery by loading the drug 5-fluorouracil (5 FU). Various weight percentages of doped 5-FU (2, 5, 7.5, and 10%) are utilized. In vitro degradation of PGS in PBS media take up to 30 days. All samples maintained their macro geometry during the degradation; after one week, they ultimately released their drugs [61].

1.5 The objective of this work

This study aims to find the best PGS scaffolds or film human cornea cell culture. To this end, the following objectives is followed"

- Synthesis, and characterization of PGS based film and scaffolds for human cornea cell culture.
- Elucidating the crosslinking mechanism of PGS
- Tuning the mechanical, optical, degradation and thermal properties of PGS according to final application

2. Chapter 2: Experimental

The Goal of the experimental part is the synthesis, characterization, characterization, and fabrication of PGS scaffolds for human cornea tissue regeneration.

2.1 Materials

PGS pre-polymers were synthesized by using glycerol (GC 99%) and sebacic acid (>99%)as monomers obtained from Merck, toluene (HPLC 99.9%) purchased from Sigma Aldrich as the solvent, and Sulfuric acid (95 to 98 %) purchased from Isolab as the catalyst.

2.2 Synthesis

Fig 12a shows the designed setup for PGS synthesis. Two-neck round-bottom flask is connected to a condenser and Dean-Stark receiver. Polymer is synthesized in different temperatures and durations to find the best processability. Table 1 indicates the different samples' synthesized conditions. The reaction stopped according to criteria: the collected water and the physical appearance (gelation point). The best result was achieved where 0.1 M of sebacic acid was mixed with 0.105 M of glycerol (5% in excess) in 70 mL of toluene. The reaction takes place at 110 ℃. The silicone bath is heated up to 150 ℃ to reach the proper reaction condition. After dissolving the sebacic acid in toluene at 90 °C, 9 μL of sulfuric acid was added to the solution as a catalyst. The reaction mixture was refluxed at varying times (50, 75, and 105 minutes) (see Fig. 12 b). The synthesized pre-PGS precipitated after cooling the reaction mixture to room temperature (RT). Since sebacic acid is insoluble in toluene at room temperature, the glycerol is added in excess to consume all sebacic acid. In the end, the pre-PGS. The precipitated pre-polymer was double washed with fresh toluene twice (20 mL) and freeze-dried for three days.

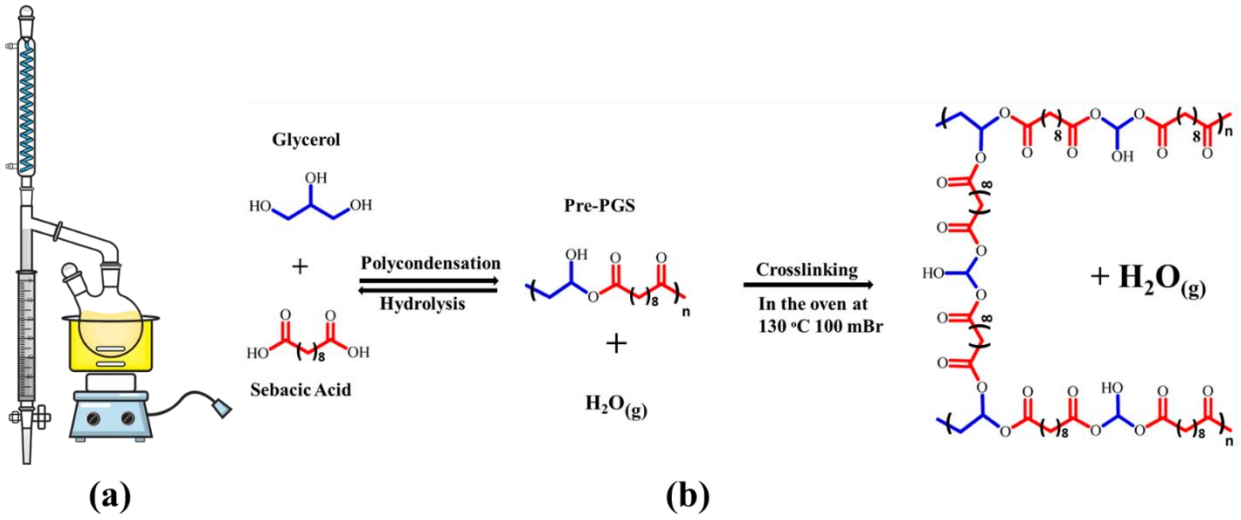

Figure 12 (a) setup of synthesis; round bottom flask connected to a condenser and a stark dean receiver in a placed silicon an oil bath. Coldwater circulation is employed for condensing the reaction vapor (b) PGS polymerization and crosslinking reactions.

Table 1 synthesis condition of different pre-PGSs the synthesis stopped in 3 different stages (i) before gelation (BG), (ii) right after gelation (RAG), and (iii) after gelation point

No of sample	Starting material ratio (G/S.A)	Oil bath temperature (°C)	Degree of crosslinking	Collected water (ml)	Duration of reaction (min)	Comments
1	1:1	150	BG	2.9	70	
2	1:1	155	RAG	1.5	180	
3	1:1	150	RAG	3.1	190	
4	1:1	145	RAG	2.2	180	
5	1:1	160	AFG	2.4	220	40 mins after GP, stopped
6	1:1	150	BG	2.9	90	
7	1:1	160	BG	2.6	60	
8	1:1	160	RAG	2.6	170	

9	1:1	150	RAG	3.5	170	
10	2:3	150	RAG	3.2	65	Solid polymer

2.3 Shaping and Crosslinking process

the obtained pre-polymer is a viscous shapeless liquid. The pre-PGS was heated up to 70 ^{o}C to lower the viscosity for ten minutes. Then, the film of pre-PGS on the aluminum foil (cleaned by IPA) is prepared by a Dr. blade at the thickness of 300 microns (see Fig.). Later, the polymer is crosslinked at 130 ^{o}C and 100 mbar at various durations, according to the final applications. For this research, three different molecular weights of pre-polymer were synthesized with different durations, 50 (PGS1), 75 (PGS2), and 105 (PGS3) minutes of synthesizing process. Later, each batch of polymer is crosslinked for 1, 3, 6, 9, 12, 24, and 48 hours to investigate the crosslinking process and its effect on the optical properties.

Figure 13 the Dr. blade adjustable film castor/coater. The thickness of film range from 10 microns to 3500 microns.

2.4 Characterization of pre-polymer and polymeric membranes

2.4.1 FTIR

The Thermo Fischer Nicolet™ iS™ 10 Spectrometer is used for ATR FTIR measurements. The films are placed on a single crystal with light pressure. Since the pre-PGS is liquid, pre-PGS droplets are placed on the single crystal. After collecting the background, the FTIR spectrum is carried out. The experiments have been conducted in the roam temperatures. Nitrogen gas flow is purged into the FTIR setup to reduce the noise.

2.4.2 UV vis spectroscopy

Agilent Cary 6000i UV-Vis-IR Spectrophotometer analyzes the PGS films' transparency. As-prepared PGS films are used directly for the measurements. The reference is the air, and the films are attached to a metallic holder with a 10 mm by 20 mm void. The wavelength range is between 800 nm to 200 nm.

2.4.3 ^{1}H NMR

Bruker Avance III 400MHz NMR spectrometer is used for NMR analysis. The pre-PGSs are dissolved in d-chloroform with a 3% concentration. Lock and shimming settings were made according to the d-solvent used before the analysis.

2.4.4 Refractive index

ATAGO Nar1T- solid is used to measure the refractive index of PGS films. The light source is LED (approximating the D-Line wavelength), and the setup was calibrated with distilled water before experiments. All analysis was measured at room temperature.

2.4.5 XPS

The "Thermo Scientific K-alpha X-ray Photoelectron Spectrometer" is employed for XPS analysis of PGS films. The photon energy of 1486.7eV (monochromatic Al Kα X-rays) at 12 kV and 6 mA with a spot size of 400 μm and an angle was 30^{o} was applied, and the collection angle was 60^{o}. During the analysis, a flood gun was used with an X-ray gun for charge neutralization on the surface.

2.4.6 GPC

Agilent 1200 Series Gradient HPLC System with polystyrene standard and PLgel 5um mixed-C 300x7,5mm column analyzed the pre-PGS molecular weight. The refractive index detector (RID) was utilized for detection. The samples were dissolved in dimethylformamide with a 1% concentration, and 20 μL of each sample was injected with a flow rate of 0.6 ml/min.

2.4.7 Differential Scanning Calorimetry (DSC)

The utilized DSC setup for this research is Thermal Analysis MDSC TAQ2000. 4 to 10 mg of dried pre-PGSs were encapsulated in an aluminum pan. The experiment is carried out under inert gas at a flow rate of 25 mL.min-1, and the working temperature is between -50 °C to 80 °C. The cooling and heating rate is 10 °C/min, and the interval between each step is 1 minute.

2.4.8 Tensile strength

Tensile strength is measured by the ESM303 series of Mark-10 company by Series 5 advanced digital force gauge. The samples are cut into 10 by 40 mm rectangular shapes. 0.2 N steps apply the force. The thickness of samples is around 200 to 250 microns.

2.4.9 Contact angle

The contact angle of PGS is measured by ----- as a value to investigate the hydrophilicity of films. 5 µl of distilled water is dropped on the PGS films, and the contact angle of water droplets on both sides after 30 seconds is measured.

2.4.10 TGA

Thermal behavior of pre-PGS is investigated by STA of Netzsch, 449 C model. 0.5 g of PGS is placed in an Alumina crucible, and the mass change is measured with another alumina crucible as a reference. The heating rate was set at 10 °C/min. The applied temperature range is from room temperature to 1100 °C.

2.5 Electrospinning

Electrospinning is a straightforward versetile technique for the fabrication of nanofiber-based mats. It has a wide application in bioengineering, textile, composite fabrication and etc [41,62].

2.5.1 Ink preparation

For electrospinning, the solvent should be polar to carry the applied voltage, and accordingly, N, N-Dimethylformamide (DMF) is used as the solvent. PGS is mixed with PCL in three different ratios (3 to 1, 1 to 1, and 1 to 3), and from each mixture, three different solutions are prepared 10, 20, and 30 weight percent (see table 1). Each solution was mixed over a night under vigorous stirring, and before E-spinning, the solution was heated up to 80 ^{o}C to homogenize the solution and complete dissolving.

Table 2 1 indicates the concentration and PLA/PGS ratios of each ink pre; the 20 percent solution with the 1 to 1 solid ratio has been successfully electrospun

Solid ratio of PLA to PGS (gr/gr)	**Concentration Solid to liquid (gr/gr)**	**E-spinning status**	**Concentration Solid to liquid (gr/gr)**	**E-spinning status**	**Concentration Solid to liquid (gr/gr)**	**E-spinning status**
3 to 1	30	Too viscose	20	splash	10	Spray
1 to 1	30	Too viscose	**20**	**successful**	10	Spray
1 to 3	30	Not applicable	20	splash	10	Not applicable

3. Chapter 3: Result and Discussion

According to the Fischer-Speier esterification mechanism (Fig 1b), the esterification reaction is reversible. Thus, water should be removed from the flask to reach a higher degree of polymerization. For this purpose, toluene is utilized as a solvent, the boiling temperature of which is 110 ^{o}C. It is also more than the water's boiling temperature; the produced water evaporates alongside the toluene, and both condense in the dean-stark distillation receiver. Thanks to the higher density of water compared to toluene, it settles beneath the toluene. By doing so, water is removed from the system and can be interpreted as a degree of esterification. The reaction continues until the desired amount of water is collected in the dean-stark receiver.

Regarding the degree of esterification, the physical appearance of polymer can be different. At the onset of the reaction, the polymer is an almost colorless viscose liquid. After a particular time (around 120 minutes), the polymerization process reaches a gelation point level. In this state, the polymer shapes into a gel, and 3.1 mL of water are accumulated in the dean-stark receiver. The polymer gets stiffer after the gelation point until it becomes fully crosslinked. At this level, the polymer is insoluble in any standard organic solvent. Since the polymer is not processable after the gelation point, the reaction is stopped before it. Subsequently, the resulting pre-polymer was freeze-dried for an adequate time to extract the possible remaining water and toluene.

3.1 Chemical characterization

3.1.1 GPC results

The molecular weight of pre-polymers synthesized in 50 (PGS1), 75 (PGS2), and 105 (PGS3) mins were analyzed by GPC. The as-synthesized pre-PGSs were polydisperse (Fig. 14). The highest molecular weight (MW) component for PGS1 was 5463 g/mol and comprised 38% of the

analyzed sample. The PGS molecular weight and its percentile were polymerization time-dependent. The PGS2 displayed a 7024 g/mol component (63%), while the PGS3 had a 9135 g/mol component (69%). Moreover, low MW PGSs (e.g., ~600, ~1000, and ~1800 g/mol), including oligomers, were detected in the pre-PGSs (Table 3). The calculated polydispersity indices (PDI) of PGS1, PGS2, and PGS3 were 1.13, 1.43, and 1.59, respectively. They were time-dependent, increasing by reaction time (polymerization). Compared to the semi-crosslinked PGS with a PDI of 12 and semi-crosslinked PGS with a PDI of 12 [60], the PGS1-PGS3 had PDIs closer to 1, indicative of narrower molecular weight distribution [63]. The oligomers with low molecular weight (<1000 g/mol) for PGS1, PGS2, and PGS3 are 21%, 11.5%, and 10%, respectively, showing that the consumption is getting slower as the synthesis process proceeds.

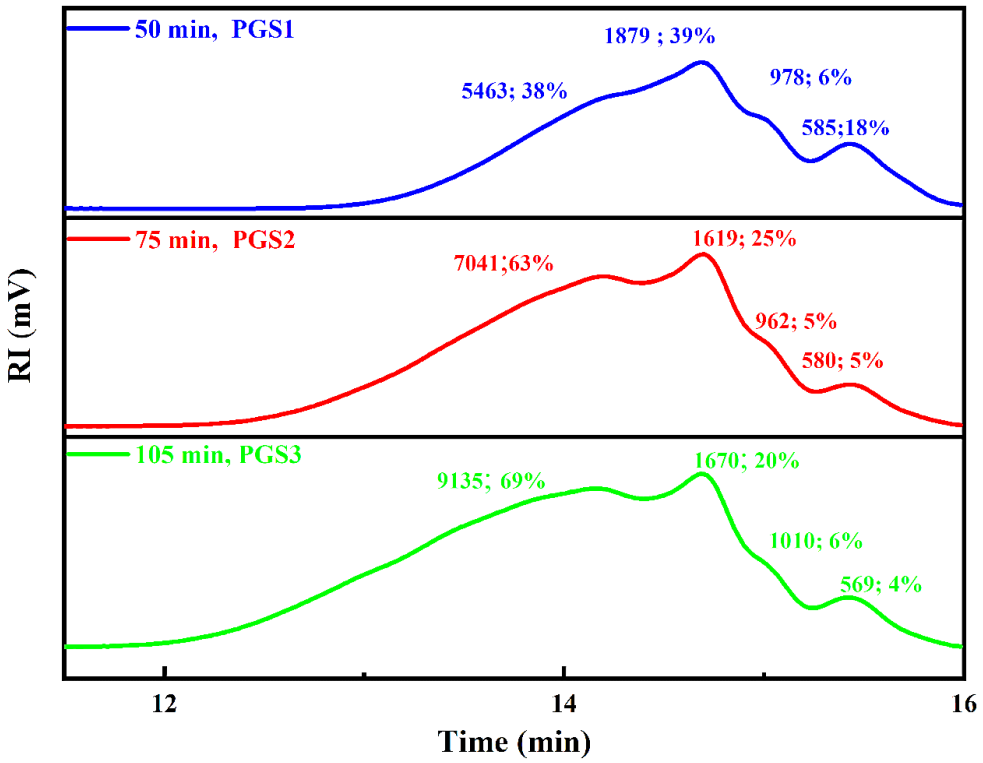

Figure 14 GPC results of three pre-polymers polymerized for 50 min (PGS1), 75 min (PGS2), and 105 min (PGS3); each peak is labeled with Mw in gram/mole with its corresponding percentage.

Table 3 GPC result of synthesized pre-polymers showing the Mw of each chain in pre-polymers with the corresponding percentage.

Sample name	Chain 1		Chain 2		Chain 3		Chain 4		PDI
	Mw (g/mol)	percentage	Mw (g/mol)	percentage	Mw (g/mol)	percentage	Mw (g/mol)	percentage	
PGS1	585	18	978	6	1879	39	5463	38	1.13
PGS2	580	5	963	5	1619	25	7041	63	1.43
PGS3	569	4	1010	6	1670	20	9135	69	1.59

3.1.2 ^{1}H NMR of pre-polymers

All pre-polymers were analyzed with 1H NMR to spotlight the structure detail. Each sample indicates chemical shifts at δ 1.30 ppm (HI), δ 1.62 ppm (HII), and δ 2.35 ppm (HIII), which corresponded to the –CO–CH2–CH2–CH2– group. These chemical shifts originated from sebacic monomers. More peaks from 3.62 to 5.08 attributed to HIV and HV plainly come from glycerol monomers [10,29]. Table 4 represents the normalized integrations of each multiplet in PGS1-PGS3 samples. The surface under each multiplet is directly related to the number of hydrogens [64]. Four CH_2 represent the H_I, assigning eight hydrogens for H_I, and the number of hydrogens in H_{II} and H_{III} is 4. The integration ratio of H_I/H_{II} and H_I/H_{III} should be 0.5, which is following table 4 values. The other integrations are also confirming the correct peak assignments. All in all, the ^{1}H NMR confirms the successful synthesis of PGS. ^{1}H NMR of PGS1 and PGS2 ar indicated in the Fig. 16.

PGS1: ^{1}H NMR (400MHz, CDCl3) Shift = 4.86 - 5.32 (1H, m, Methine (V)), 4.04 - 4.41 (19H, m, Methylene (IV)), 3.67 - 4.01 (7H, m, Methine(V_b)), 3.55 - 3.66 (2H, m, Methylene (H_{IV_b})), 2.16

- 2.45 (23H, m, Methylene (III)), 1.50 - 1.71 (21H, m, Methylene (II)), 1.31 (43H, br. s., Methylene (I))

PGS2: ^{1}H NMR (400MHz, CDCl3) Shift = 4.82 - 5.39 (2H, m, Methine (V)), 4.03 - 4.38 (16H, m, Methylene (IV)), 3.65 - 4.01 (6H, m, Methine (V_b)), 3.55 - 3.62 (1H, m, Methylene (H_{IV_b})), 2.20 - 2.43 (17H, m, Methylene (III)), 1.61 (17H, d, J = 6.9 Hz, Methylene (II)), 1.30 (33H, br. s., Methylene (I))

PGS3: ^{1}H NMR (400MHz, CDCl3) Shift = 4.87 - 5.32 (1H, m, Methine (V)), 4.04 - 4.39 (20H, m, Methylene (IV)), 3.66 - 4.03 (7H, m, Methine (V_b)), 3.54 - 3.65 (2H, m, Methylene (H_{IV_b})), 2.18 - 2.46 (22H, m, Methylene (III)), 1.61 (22H, d, J = 7.0 Hz, Methylene (II)), 1.30 (45H, br. s., Methylene (I))

Table 4 ^{1}H NMR integrations of each samples specified multiplets.

Multiplets	**Normalized Integration of PGS1**	**Normalized Integration of PGS2**	**Normalized Integration of PGS3**
Methylene (H_I)	1	1	1
Methylene (H_{II})	0.489721	0.485884	0.489476
Methylene (H_{III})	0.529243	0.492942	0.498762
Methylene (H_{IV_b})	0.052112	0.053816	0.051176
Methine (V_b)	0.16255	0.613366	0.165497
Methylene (IV)	0.441434	0.047861	0.449649
Methine (V)	0.015936	0.04367	0.020636

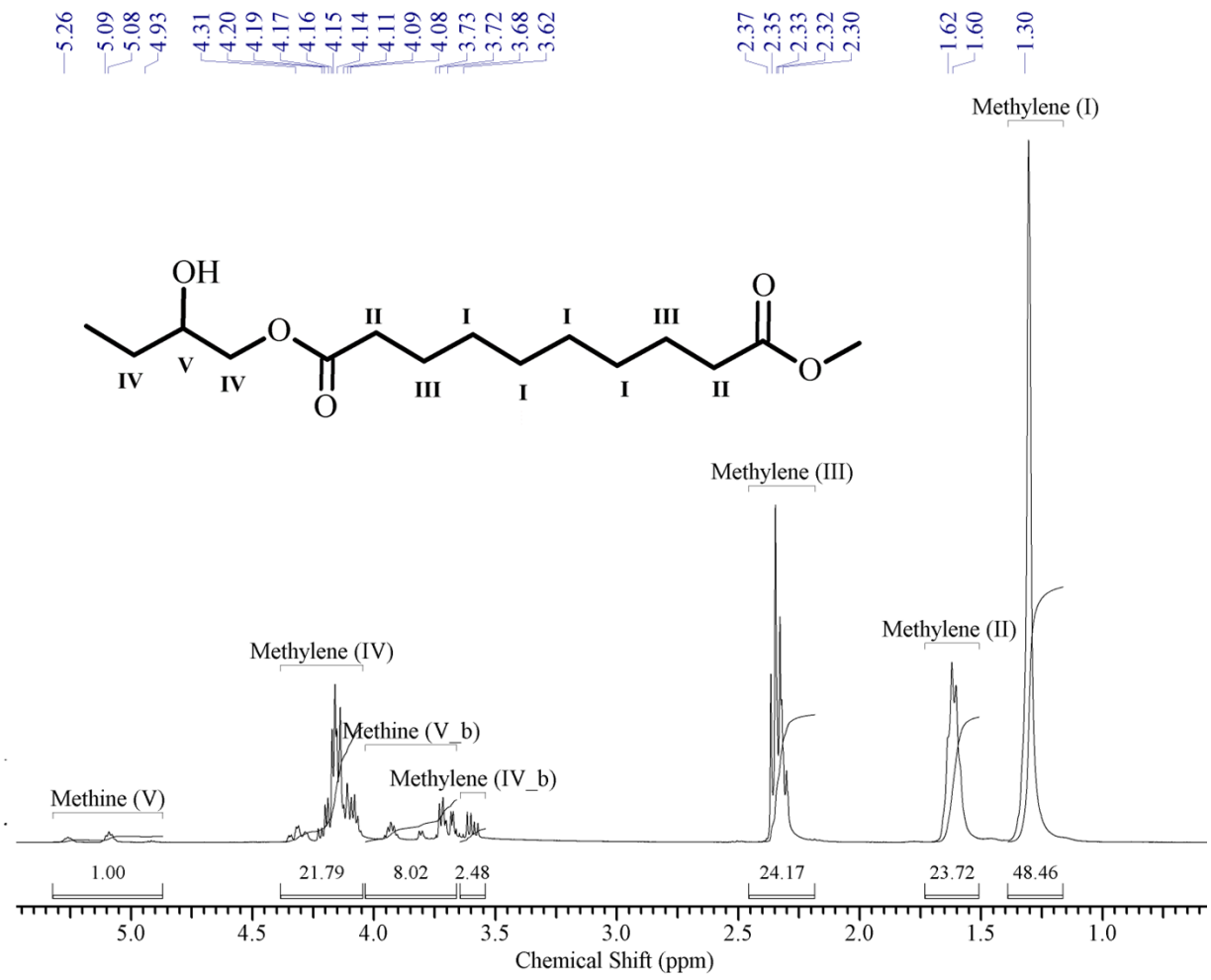

Figure 15 ^{1}H NMR spectra of PGS3 indicating the assigned hydrogen multiplets and their integrations.

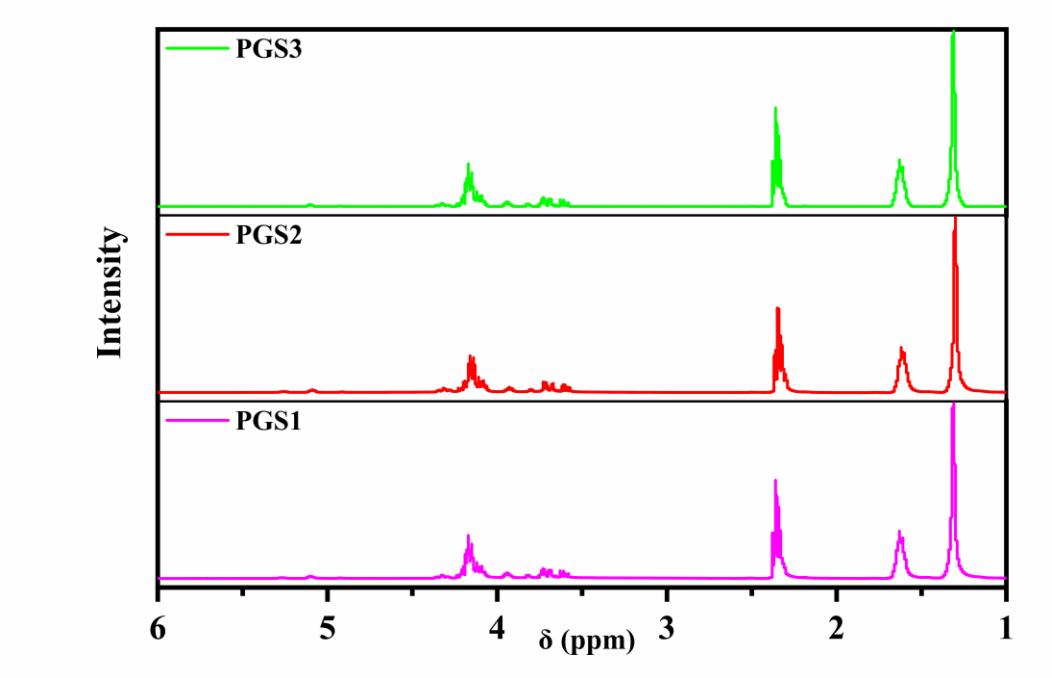

Figure 16 1H NMR of all three samples.

3.1.3 FTIR

FTIR confirmed the successful synthesis of pre-PGSs. PGS1-PGS3 (Fig. 17 a1, b1, and c1) displayed a very sharp peak at 1733 cm-1, ascribed to the C=O stretching of the ester functional groups. Also, two peaks at 2884 and 2927 cm-1 were attributed to the C-H stretching. Moreover, the broad peak at 3000-3600 cm-1 was ascribed to primary and secondary alcohol hydroxyl groups and the acid end groups. More importantly, there was a typical peak at ~1703 cm-1 for all pre-polymers, corresponding to the C=O stretching of the acid end groups (see Fig. 17 a2, b2, and c2). Comparing three pre-PGS spectra indicates three main differences: consumption of OH bond and C=O bond in the acid end group and increasing the C=O bond in the ester function. The ratio of the height of the C=O peak in the acid end group and OH bond peak to the highest peak (C=O in the ester linkage) are 0.956 and 0.203 for PGS1, 0.928, and 0.199 for PGS2, and 0.912 and 0.188 for PGS3, respectively. Clearly, the esterification continues as the synthesis goes on.

During crosslinking, the FTIR spectra of each batch have undergone the exact three main changes, only this time intensively (see Fig. 17 b and c columns). The OH bond and the C=O of the acid end group were consumed, and the relative transmittance of the C=O peak in the ester linkage was increased in three molecular weights (see Fig. 17, second and third columns). These changes imply that acid end groups or remaining acid connect with secondary and primary alcohol and link the PGS chains. Furthermore, as the chain length of pre-PGS increases, the rate of consumption of acid end groups and OH bonds reduce. Fig. 17 a2 shows that acid end groups are consumed much faster compared to the samples in Fig. 17 b2 and c2. The same scenario is also valid for OH bonds (see Fig. 17 a3, b3, and c3). This can be related to the high mobility of polymers with small chains. The same peak positions and changes during crosslinking have been reported by Israd H. Jaafar et al. [25] and Chi Ching Lau et al. [10].

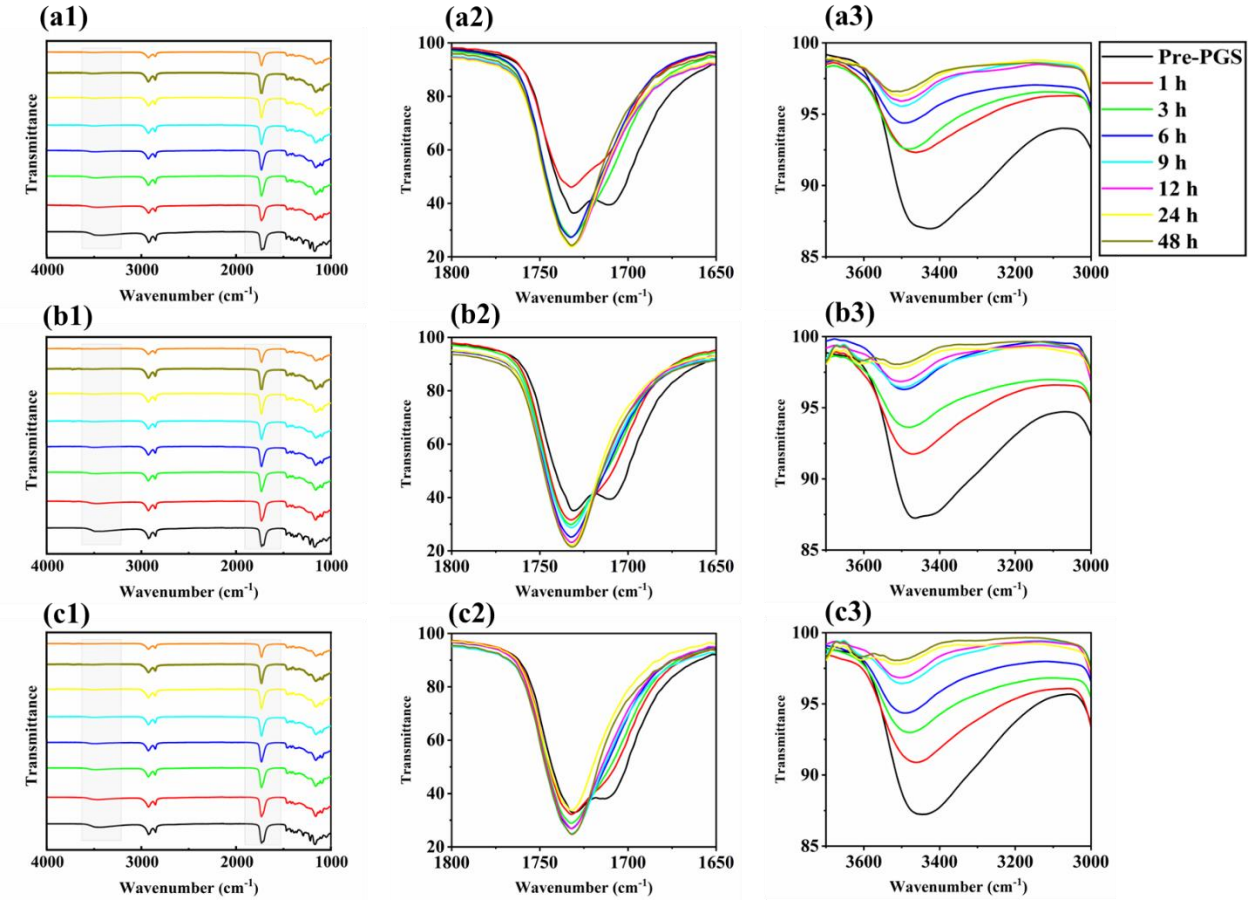

Figure 17 FTIR spectra of three pre-polymers crosslinked in the different durations. Alongside the whole spectrum (A1, B1, and C1), the 1850-1600 nm region is enlarged to show C=O bonds, and the 36500-3000 nm region is enlarged to show OH bonds. (A1) FTIR spectrum, (A2) C=O bond, and (a3) OH Bond of PGS1 samples(B1) FTIR spectrum, (B2) C=O bond, and (B3) OH Bond of PGS2 samples (C1) FTIR spectrum, (C2) C=O bond, and (C3) OH Bond of PGS3 samples is shown.

3.2 Thermal analysis

Thermal analysis of PGS is investigated by DSC and TGA to elucidate the related properties.

3.2.1 TGA

TGA of PGS2 was recorded to evaluate the degradation behavior (Fig. 18). Till 220 °C, there was no significant change in the polymer's weight. Around 3 percent of change may be related to absorbed water. From around 250 °C, degradation starts, around 380 °C sharply increases, and after 600 °C, all PGS decomposed.

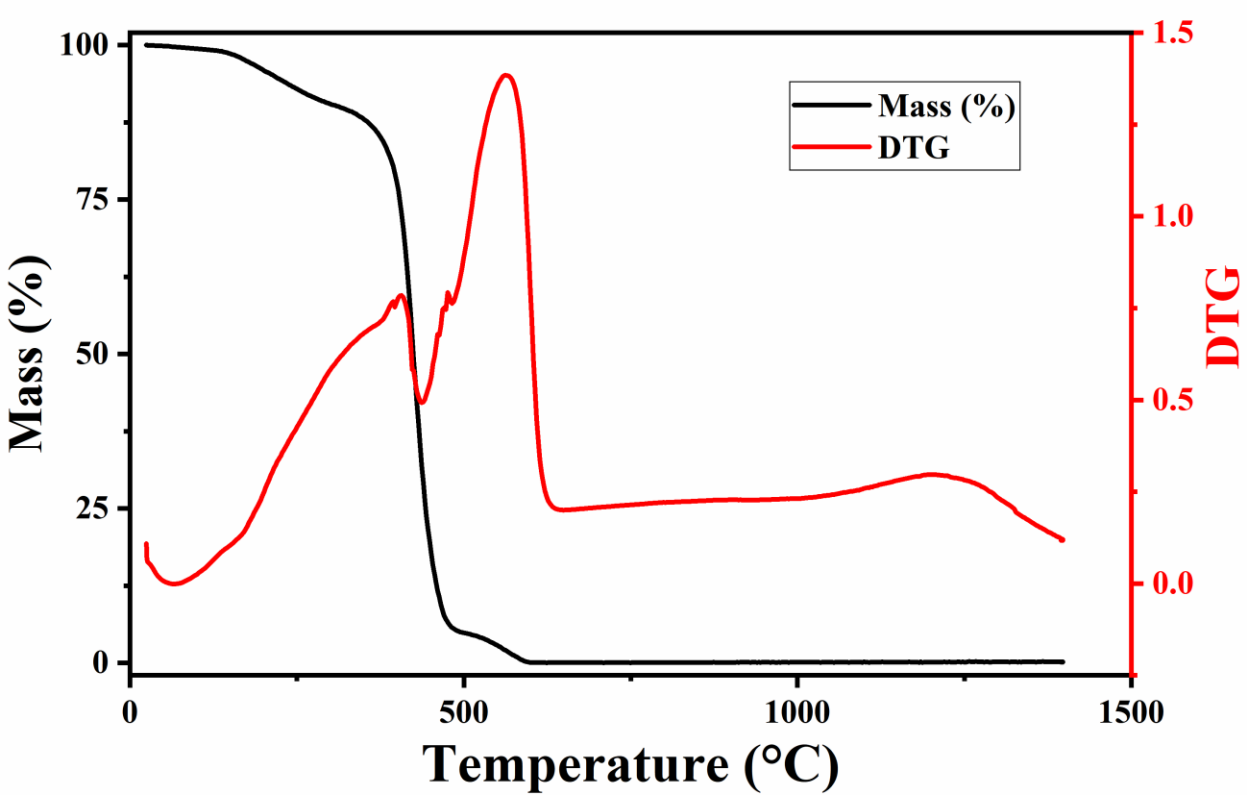

Figure 18 TGA of PGS2

3.2.2 DSC

DSC has analyzed three samples with different molecular weights to investigate PGS's thermal and crystallographic properties. In Fig. 19, the second curve of each sample is indicated to eliminate the possible thermal history by melting the polymer. The rate of cooling and heating was 10 °C/min. Additionally, the crystallization enthalpy of each sample labeled on the graph indicates the amount of crystalized phase. The values of each sample are tabulated in table 5. PGS1, with the lowest molecular weight, indicated the highest crystallization enthalpy (58 J/g), meaning the highest crystallization. This could be due to small chain mobility in rearranging themselves to crystallize. The PGS2 and PGS3 samples indicated 42 J/g and 20 J/g crystallization enthalpy, respectively, confirming the high mobility of small chains. PGS is a semicrystalline polymer, and

each sample showed a Tg step, in which the position did not change significantly with molecular weight.

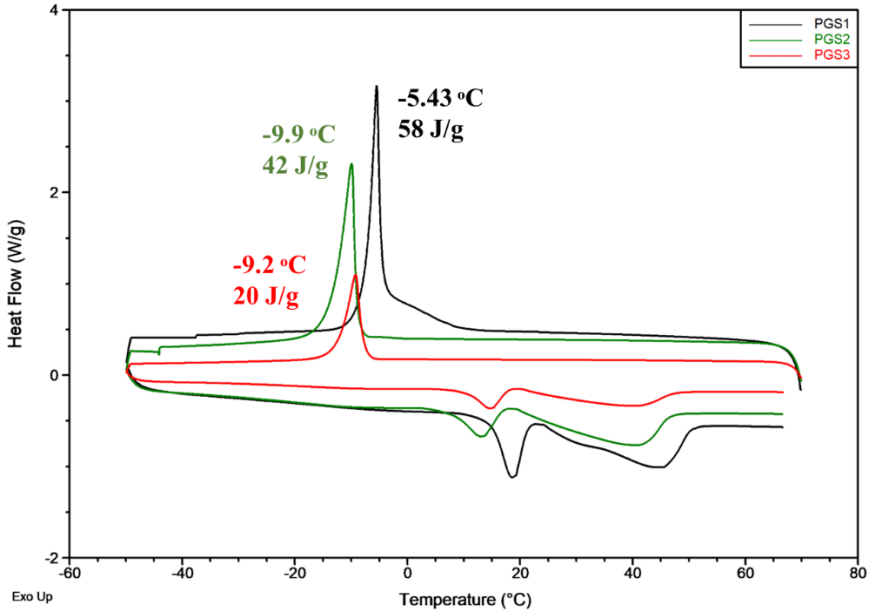

Figure 19 DSC curves (second curve) of PGS1-PGS3 with their crystallization enthalpy. PGS1, due to low molecular weight and higher molecules' mobility, showed higher crystallization

Mobility of chains also affected the melting and crystallization behavior of PGS. Long chains need more time and enthalpy to change their phase from liquid to solid or vice versa. Crystallization temperature has shifted from -5 °C to -9 °C, and the highest limit for melting range has shifted from 51 °C to 53 and 57 °C as molecular weight increased.

Table 5 calculated value thermal values for each sample by TA analysis software for PGS1-PGS3.

Samples	**Tg range (°C)**	**Crystallization Temperature (°C)**	**Crystallization Enthalpy (J/g)**	**Melting range (°C)**
PGS1	-18 to -12	-5	58	13 to 51
PGS2	-20 to -12	-9.9	42	10 to 53
PGS3	-22 to -10	-9.2	20	12 to 57

3.2.3 Contact angle

Fig. 20 shows contact angles of the PGS2 sample crosslinked for 12 and 24 hours. The contact angle of 12 hours of crosslinked polymer is 61 degrees (Fig 20a), and that of 24 hours of crosslinked polymer is a little higher, which is 67 degrees (Fig 20 b). As shown in the FTIR spectrum PGS (see Fig. 17 b3), OH is consumed during the crosslinking. Thus, the 12 crosslinked sample has a broader OH peak than the 24-hour crosslinked sample. OH is a hydrophilic function, and the abundant presence in less crosslinked samples results in hydrophilic films.

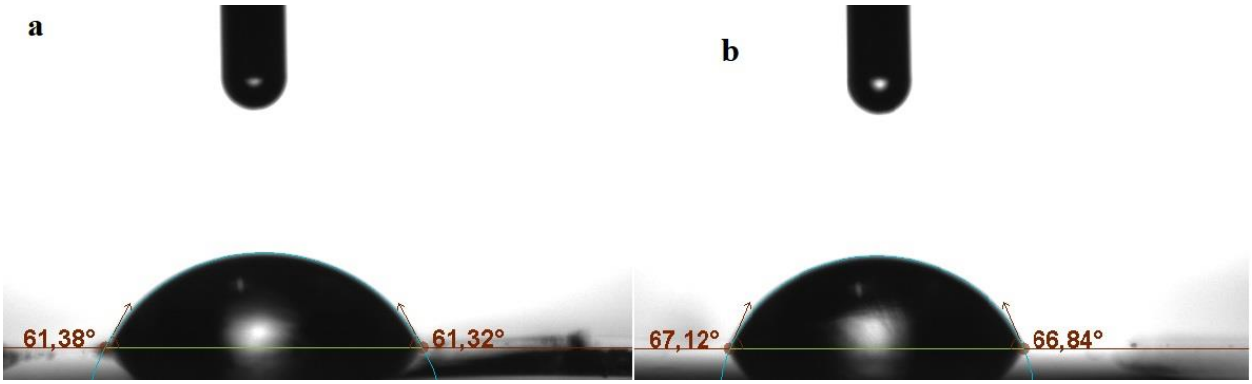

Figure 20 Contact angle of PGS2 crosslinked for 12 hours (a) and 25 hours (b).

3.3 Mechanical properties

So many studies have widely investigated the mechanical properties of PGS. Accordingly, in this study, we have measured only two different samples crosslinked for 12 and 24 hours. The cross-section of samples is 10 mm by 200 to 220 microns. From each PGS, five samples are cut with sharp blasé to avoid any cracks as much as possible. Fig. 18 shows the stress-strain curve one of each set as a representative. In 24-hour crosslinked PGS, the tensile strength at break is 0.42 MPa,

and the strain at break is 0.04%. However, the tensile strength at break of 12-hour crosslinked PGS is 0.2 MPa, and the strain at break is 0.09%. Due to the formation of the 3d network of PGS as crosslinking continues, the strength of PGS increases in the price of losing elasticity.

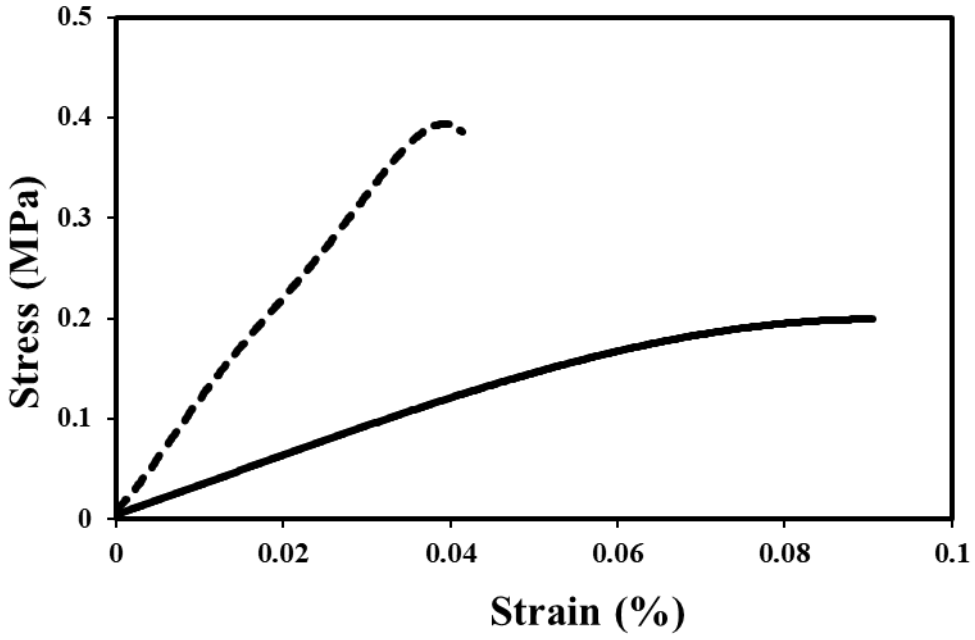

Figure 21 the stress vs. strain graph of 12 (straight line) and 24 hours-crosslinked (dashed line) samples

3.4 Optical properties of PGS films

This research aims to use the PGS as a scaffold for human cornea tissue regenerations. Thus, the optical properties of PGS are a crucial factor that should be tuned according to the final application.

3.4.1 UV-vis spectroscopy

Bare PGS films that are crosslinked for 1 hour transmit more than 80 percent of visible light and near UV spectra (Fig. 18 a), whereas the 25-year human cornea transmits just 60 percent of the

visible light (Fig. 22 b) [65]. Even PGS films crosslinked for 23 hours indicate better performance than the old-aged human cornea. The films crosslinked for 1-hour exhibit absorption in the middle UV range (300 to 200 nm). As the synthesis reaction time increases, the light absorbance of 1-hour crosslinked PGS films exhibits a redshift in the UV vis spectroscopy. Still, placing the abortion onset in the visible light spectrum is not significant enough. However, in the 24-hour crosslinked PGS in all three molecular weights, the absorption starts at the visible light spectrum, causing the PGS films to have a color.

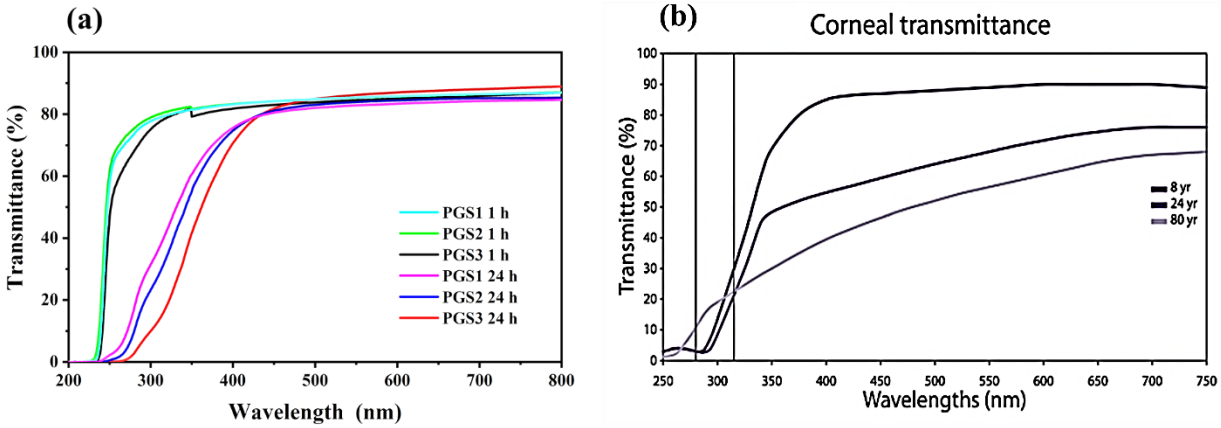

Figure 22 UV vis spectroscopies of (A) synthesized polymer batches crosslinked in different durations and (b) human cornea at different ages adapted from [65].

Overall, Fig. 22 indicates that the polymerization and crosslinking process affect the optical properties of PGS, and it needs further investigation to spotlight it. Yet first, the PGS chromophore should be discussed. According to the chemical bonding theory and the law of conservation of orbitals, the number of orbitals created should equal the number of orbitals contributed to making those orbitals. In other words, when two atomic orbitals join together, two orbitals should be generated. Two orbitals are produced in a single bond between oxygen and carbon, σ (bonding) and σ* (antibonding). Antibonding orbital has a destructive effect of separating two atoms with covalent bonding. Clearly, when the double bond between the oxygen and the carbon is created,

two different orbitals are produced, π and π*. When an incident light passes through PGS or is scattered from its surface, it suffers from an inelastic collision. Accordingly, some of its energy is absorbed by electrons to be excited to high-energy states or orbitals. HOMO, the highest occupied molecular orbital, and LUMO, the lowest unoccupied molecular orbital, are defined by bonding and antibonding orbitals in covalently bonded materials. Fig. 23a indicates five possible electron excitations within a molecule with double or triple bonds. Due to the small amount of required energy for two of these excitations (compared to the other three transitions), only these two are in UV and visible light spectra, π to π* and n to π*. For example, σ to σ* demands a photon with higher energy than the UV-vis range. Thus, double or triple bonds are required to create color and absorption in the UV spectrum [66–68].

PGS has a double bond between carbon and oxygen in the acid endings and ester functions (Fig. 23b). Additionally, PGS has two pairs of non-boding electrons, making the n to π* transition possible. Nonbonding electrons are not shared; hence, they have higher energy than bonding electrons. Further, they do not have a destructive effect on covalent bonds, making their energy state lower than the antibonding state of energy. Therefore, the energy difference between n to π* is less than π and π*, making them the role player as energy absorbers in the UV-vis region.

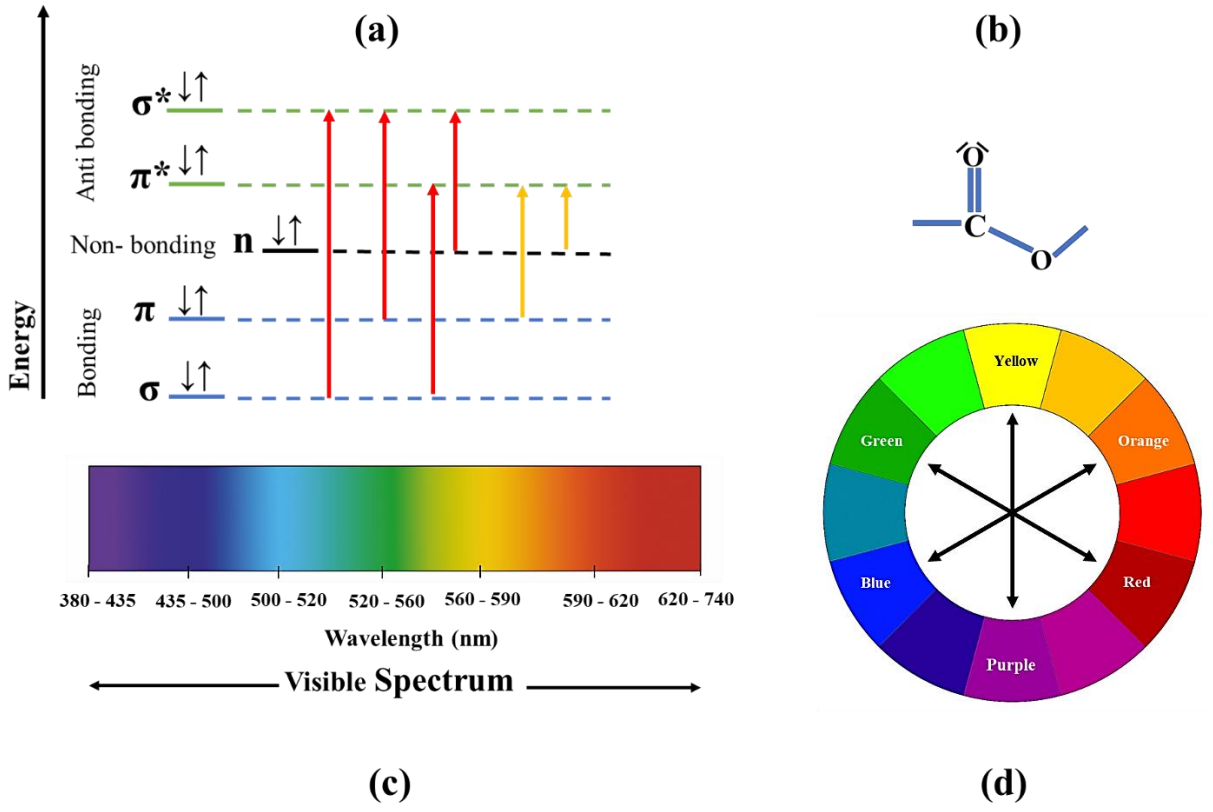

Figure 23 (A) possible transitions in the covalently bonded molecules indicate five possible excitations within a molecule with double or triple bonds. Only the orange transmissions are in the UV-vis region, π to π* and n to π* (B) COO- functional group, the chromophore of PGS (C) visible light spectrum (D) Newton's complementary color wheel; the observed color of a material is a complementary color of the region which it absorbs when visible light is reflected or passed through it.

According to Newton's complementary color wheel (Fig. 23c), when the absorption occurs at a specific color of visible light, the color we observe is the complementary color of that particular region [69]. Regarding the visible light spectrum (Fig. 23d), PGS films crosslinked for 24 hours indicate absorption in the violet region; hence, the color of these films should be yellow. The obtained PGS films have subtle yellowish color due to negligible absorption in the violet area.

To compare all three crosslinked PGS films, the normalized transmittance of UV vis spectroscopy of PGS1, PGS2, and PGS3 are presented in Fig. 24. The wavelength of each crosslinked sample at which they pass 70% transmittance is tabulated in table 5. The redshift is seen in every three molecular weights by increasing the crosslinking time. It seems that PGS films exhibit compatible

transparency to the widely used natural polymer membrane made of collagen for corneal tissue engineering, which exhibits UV-vis transmittance of 80% at 800 nm wavelength and 72 ± 5% at 400 nm wavelength [70].

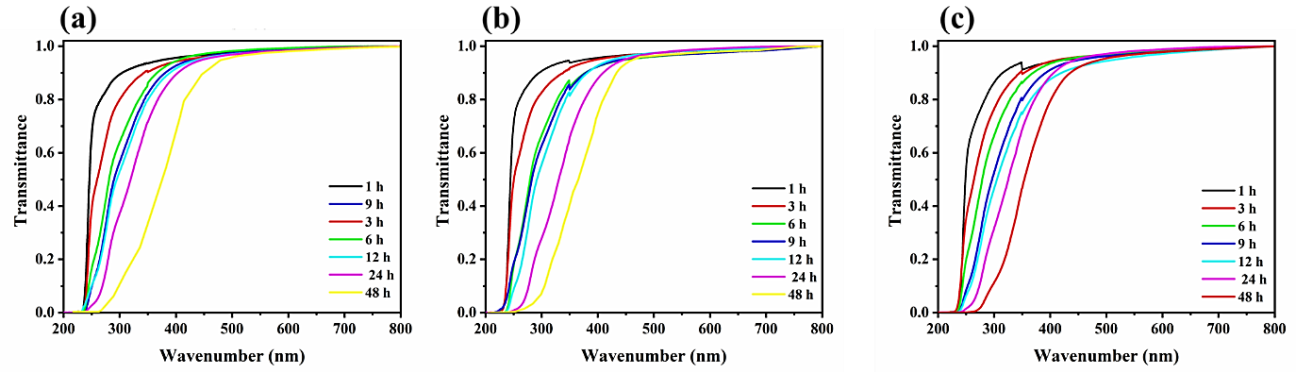

Figure 24 (a) UV vis spectroscopy of (a) PGS1 (b) PGS2, and (c) PGS3 batches crosslinked in different durations.

Table 6 shows the wavelength of each crosslinked sample at which they pass 70% transmittance.

Sample name; Crosslinking time (h)	**Wavelength (nm) at 70% transmittance**	**Sample name; Crosslinking time (h)**	**Wavelength (nm) at 70% transmittance**	**Sample name; Crosslinking time (h)**	**Wavelength (nm) at 70% transmittance**
PGS1; 1	266	**PGS2; 1**	261	**PGS3; 1**	285
PGS1; 3	303	**PGS2; 3**	299	**PGS3; 3**	307
PGS1; 6	323	**PGS2; 6**	321	**PGS3; 6**	329
PGS1; 9	347	**PGS2; 9**	335	**PGS3; 9**	355
PGS1; 12	355	**PGS2; 12**	355	**PGS3; 12**	379
PGS1; 24	382	**PGS2; 24**	383	**PGS3; 24**	381
PGS1; 48	394	**PGS2; 48**	395	**PGS3; 48**	399

3.4.2 Refractive index

The polymer's refractive index does not change significantly with molecular weight and crosslinking duration. Yet, the graph shows a logical increase in the refractive index by increasing the crosslinking degree (Fig. 25). The refractive index (RI) is repeated three times with different parts of each sample; due to the homogeneity of the samples, the results are the same, and thereby the picture has no error bars. The RI of PGS1 films starts from 1.865, crosslinked for 1 hour, ending at 1.489 when crosslinked for 48 hours. Moreover, PGS2 and PGS3 samples change from 1484 and 1.484 to 1.4898 and 1.490, respectively. As suggested in the FTIR (and later in XPS sections), the polymer with high molecular weight due to the immobility of longer chains needs more time to rearrange itself to establish cross branches. Accordingly, the rapid increase in refractive indices is observed in the lower molecular weights in the initial crosslinking stages. Since the crosslinking process is slow at PGS1, it has the lowest refractive index, and that is due to the low density of less crosslinked PGS.

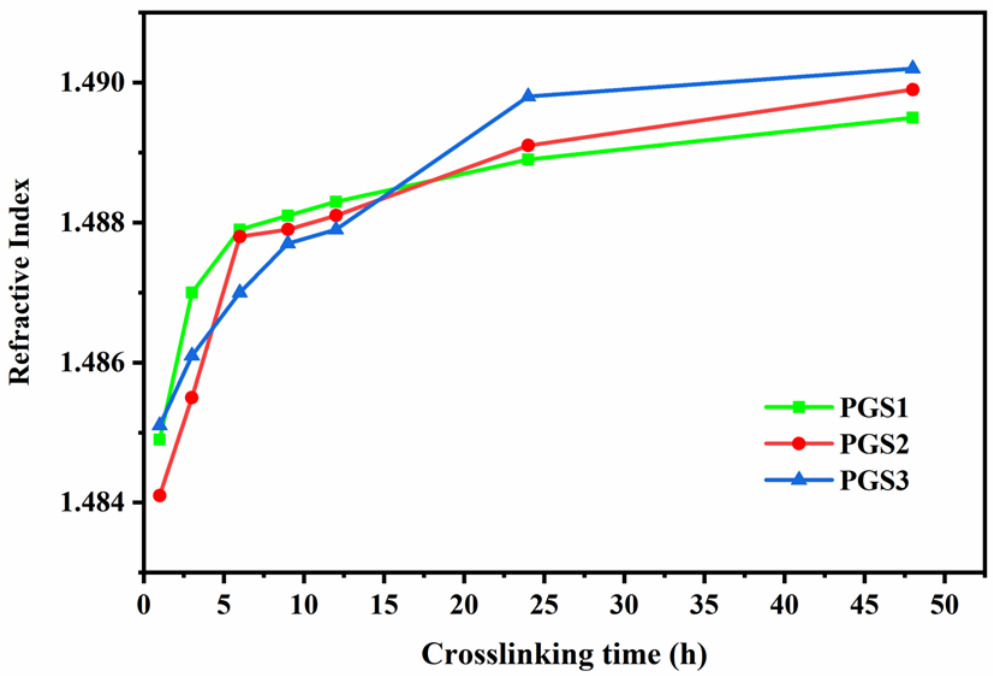

Figure 25 refractive indices of different Mw of PGS in various crosslinking hours.

3.5 XPS characterization

A characterization tool that deals with the electron binding energy was needed to deepen our understanding of the reason behind the redshift in the crosslinking process [71]. Four samples from each batch were chosen to scrutinize the electron binding energy. XPS data of 12 hours of crosslinked PGS1 film is given in Fig. 26 a to represent the whole spectrum and the deconvoluted peaks. PGS showed three deconvoluted peaks for the carbon 1s peak, representing the six types of carbons that might be found in the structure regarding binding energy status (Fig. 26b). C-C and C-H peaks are found at around 385 eV, C-O peak at around 386.4 eV, and C-OH peak at around 389 eV. There is also a tale shape peak around 289 eV ascribed to the COO- group as an ester function or acid end group. As discussed, due to a double bond in the ester function, the tale is suggested to be the chromophore site of PGS.

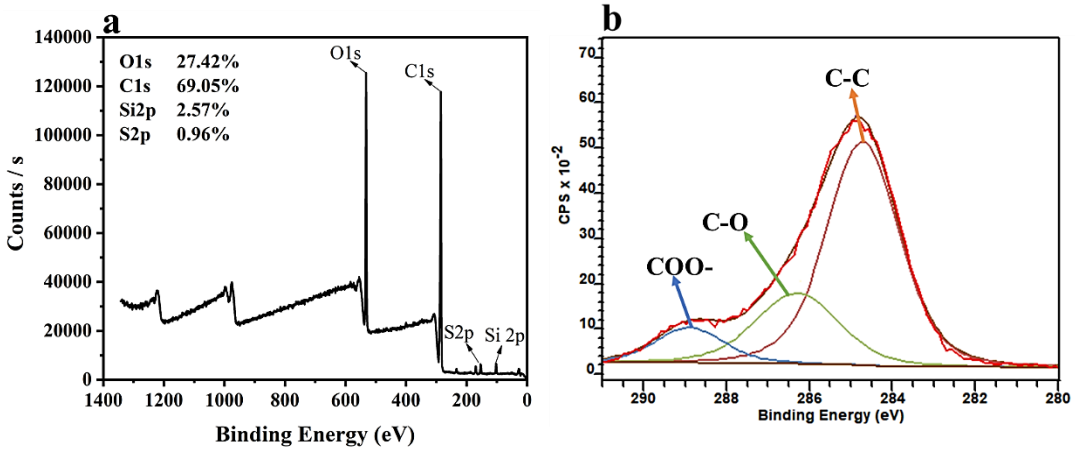

Figure 26 XPS result of PGS1 batch crosslinked for 12 hours (a) the whole spectrum (b) the Carbon 1s peak and its deconvoluted peaks.

When the carbon 1s XPS results of all samples are compared, the tale peak, which was more dominant at the initial stages of crosslinking, is apart from the C-C and C-O convoluted peaks. As the crosslinking proceeds, the tale joins to the bigger peak (see Fig. 27a to c). When the deconvoluted positions of the COO- group in the carbon 1s peak for three molecular weights were compared (Fig. 27d), a noticeable peak shift towards smaller binding energy was observed for all samples. COO- function binding energy was shifted from 289.05 eV to 288.79 eV in PGS1, from 289.12 eV to 288.8 eV in PGS2, and from 289.16 eV to 288.6 eV in PGS3. This could be because the electrons in the carbon need less energy to be excited from the 1s orbital to the higher energy. This data is consistent with UV-vis spectroscopy finding where the electrons require less energy to be excited to the antibonding orbitals as the crosslinking proceeds, and the electrons in the carbon atom in the ester function get excited with violet light. In addition, when carboxylic acid loses its single hydrogen atom and joins another chain, the gap between HOMO and LUMO is affected by the whole chain on two sides [71,72].

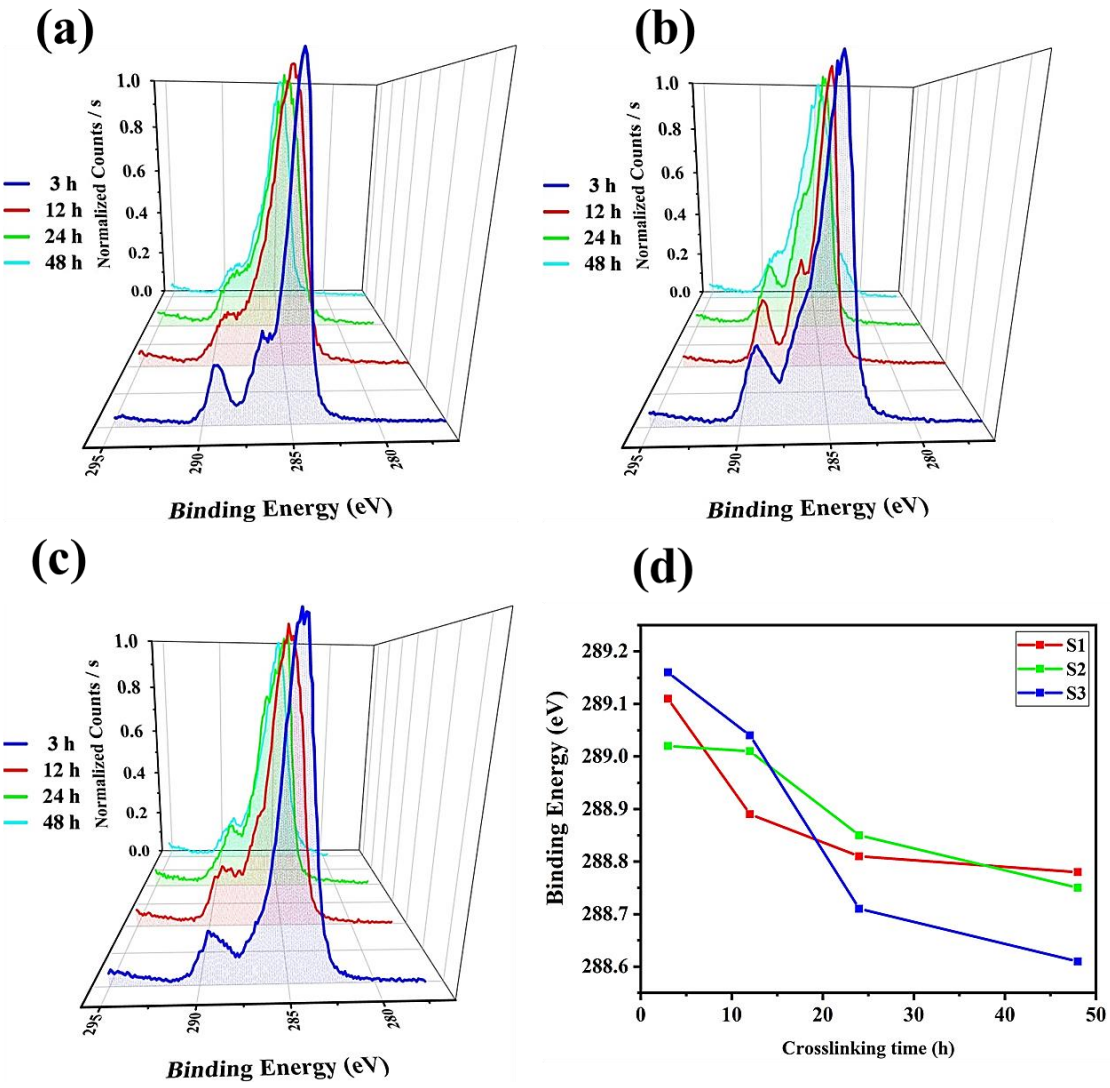

Figure 27 normalized XPS result of carbon 1s of (a) PGS1, (b) PGS2, and (c) PGS3, and (d) the deconvoluted positions of the COO- group in the carbon 1s peak for three molecular weights.

The reason behind the found shifts towards smaller energy in XPS and UV-vis spectroscopy lies in the crosslinking mechanism. As shown in Fig. 12 b, the acid end groups of pre-PGS chains connect with secondary OH on the backbone. The hydrogen in the carboxylic acid reacts with the OH to crosslink two polymeric chains, generating water as the byproduct. The water evaporates in the vacuum oven at 130 ^{o}C. To be specific, the single-bonded oxygen in the O=C-OH group breaks the bond with the hydrogen, has an electronegativity of 2.2, and connects with the carbon in the backbone with an electronegativity of 2.5. The increase in the electronegativity of the adjacent

atom reduces the density of electrons on the atom, emitting the photoelectron, which lowers the binding energy of electrons [71]. The adjacent carbon is more electronegative than hydrogen, reducing the power of the oxygen in the ester group, thereby, the carbon electrons are less bound to ester function, and they demand less energy to be excited to higher states. Expressly, as crosslinking progresses, the absorption energy of electrons of carbon in the ester group undergoes a redshift from middle range UV to violet spectrum.

The other intriguing issue in the XPS results confirms the assumption in the second and third columns of Fig. 17 that longer chains have less mobility than short chains and cannot reposition themselves to crosslink. Thus, the crosslinking is slow at higher Mw. Fig. 27d indicates that the PGS3 batch (highest Mw) has the highest binding energy at the first twelve hours of crosslinking. Still, after the end, it shows the lowest binding energy. Moreover, after 24 hours of crosslinking, all samples reached a saturation point, and the rate of changes was smoothed. Interestingly, the refractive index of PGS films has a similar path to the COO binding energy- as in Fig. 27 d and Fig. 25.

3.5.1 Effect of cell culture on optical properties

Fig. 28 indicates the UV-vis graph of 48-hour crosslinked PGS films seeded with retina and human cornea epithelium cells. There is no significant change in the optical properties in the films with higher molecular weights. The optical properties of cultured films are tabulated in Table 6. In the film with the highest molecular weight of pre-polymer, PGS3, the wavelength that transmits 70% of the incident in the bare film (PGS3_B) is 398 nm increasing to 425 nm in film cultured by epithelium (PGS3_E) and to 410 nm in film cultured by Retina PGS3_R. In PGS2 and PGS3 films, these changes are more significant. The wavelength that transmits 70% of the incident for PGS2 has increased by 40 nm for PGS2_E and 130 nm for PGS2_R. For PGS1, the number increased by

154 nm and 260 nm after being cultured by epithelium and retina, respectively. The refractive indices did not change significantly after being cultured. The refractive index of PGS1 – PGS3 films is around 1.485 showing an insignificant reduction.

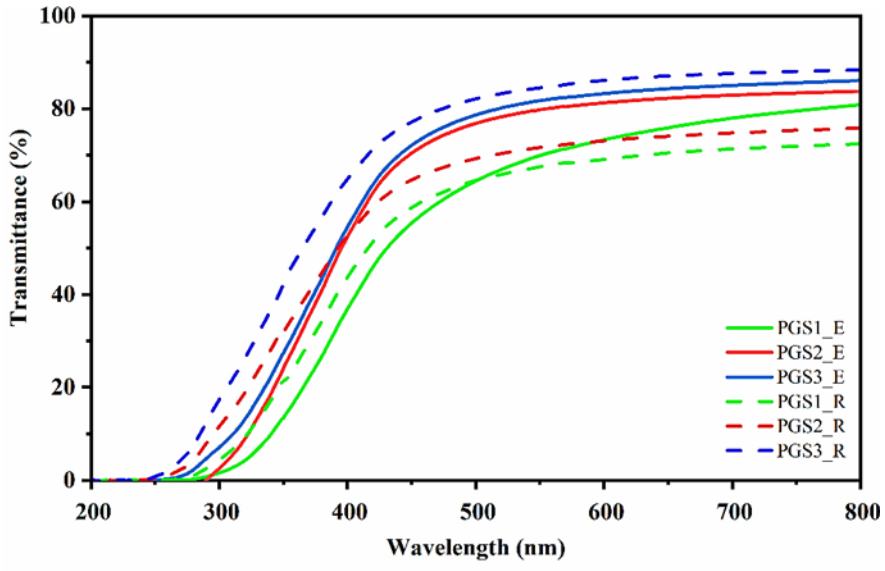

Figure 28 UV-vis spectroscopy of seeded PGS1-PGS3 films crosslinked for 48 hours with epithelium and retina cells.

Table 7 optical properties of bare and cultured PGS1-PGS3 films crosslinked for 48 hours.

Sample name	**PGS1_ B**	**PGS1_ E**	**PGS1_ R**	**PGS2_ B**	**PGS2_ E**	**PGS2_ R**	**PGS3_ B**	**PGS3_ E**	**PGS3_ R**
Refractive index	1.489	1.486	1.4852	1.4898	1.485	1.485	1.49	1.4856	1.4858

Wavelength (nm) at 70% transmittance	394	550	660	395	430	530	399	425	410

4. Conclusion

The optical properties of PGS polymer have been investigated by UV-vis spectroscopy and the Refractometer. Bare PGS indicates better transparency than the human cornea. The bare low-molecule PGS films have about 80% transmittance at 800 nm and around 70% at 400 nm. As crosslinking proceeds, the PGS films acquire light yellowish color due to absorption in the violet region. As discussed earlier, the chromophore site of PGS is the ester function Due to the presence of a double bond. This paper suggests that the cause of the formation of color lies in the crosslinking mechanism. FTIR and UV-vis data confirm that as the crosslinking proceeds, the ester function's carbon electrons get excited with less energy, whereby they can absorb visible light alongside UV light. In the crosslinking process, acid end groups connect with more electronegative atoms and lose their power to control the electrons. For example, in the PGS3 sample (having the highest pre-polymer molecular weight among others), in the 3-hours crosslinked PGS films, the carbon 1s electrons have 298.15 eV binding energy; however, after crosslinking for 48 hours, this number lowers to 188.6 eV. The same samples also suffer from a reduction in the binding energy as the crosslinking progresses. The refractive index of PGS polymers did not show a significant difference by changing the polymerization and the crosslinking process. Still, it followed a rational path. The refractive index of PGS films changed from 1.487 to 1.489. This research provides data that can help researchers tune the PGS properties according to the final applications by the polymerization and crosslinking process. Moreover, it allows researchers to deepen their knowledge about PGS crosslinking process.

5. References

[1] B. Dhandayuthapani, Y. Yoshida, T. Maekawa, D.S. Kumar, Polymeric Scaffolds in Tissue Engineering Application: A Review, International Journal of Polymer Science 2011 (2011) 1–19.

[2] M.I. Sabir, X. Xu, L. Li, A review on biodegradable polymeric materials for bone tissue engineering applications, J Mater Sci 44 (2009) 5713–5724.

[3] H.-J. Endres, Engineering biopolymers: Markets, manufacturing, properties, and applications, Hanser Publishers, Cincinnati, 2011.

[4] S.V. Bhat, Soft Tissue Applications, in: S.V. Bhat (Ed.), Biomaterials, Kluwer Academic, Boston, Mass., London, 2002, pp. 112–129.

[5] Y. Lin, E. Bilotti, C.W.M. Bastiaansen, T. Peijs, Transparent semicrystalline polymeric materials and their nanocomposites: A review, Polym Eng Sci 60 (2020) 2351–2376.

[6] I.-L. Ngo, C. Byon, A Review on Enhancing Thermal Conductivity of Transparent and Flexible Polymer Composites, sci adv mater 8 (2016) 257–266.

[7] Young-Woo Lim, Jungho Jin, Byeong-Soo Bae, Optically Transparent Multiscale Composite Films for Flexible and Wearable Electronics, Advanced Materials 32 (2020) 1907143.

[8] S. Salehi, M. Fathi, S.H. Javanmard, T. Bahners, J.S. Gutmann, S. Ergün et al., Generation of PGS/PCL Blend Nanofibrous Scaffolds Mimicking Corneal Stroma Structure, Macromol. Mater. Eng. 299 (2014) 455–469.

[9] Y. Wang, G.A. Ameer, B.J. Sheppard, R. Langer, A tough biodegradable elastomer, Nat Biotechnol 20 (2002) 602–606.

[10] C.C. Lau, M.K. Bayazit, J.C. Knowles, J. Tang, Tailoring degree of esterification and branching of poly(glycerol sebacate) by energy efficient microwave irradiation, Polym. Chem. 8 (2017) 3937–3947.

[11] X.J. Loh, A. Abdul Karim, C. Owh, Poly(glycerol sebacate) biomaterial: synthesis and biomedical applications, J. Mater. Chem. B 3 (2015) 7641–7652.

[12] G.B. Perin, M.I. Felisberti, Enzymatic Synthesis of Poly(glycerol sebacate): Kinetics, Chain Growth, and Branching Behavior, Macromolecules 53 (2020) 7925–7935.

[13] Enzymatic polymerization of poly(glycerol-1,8-octanediolsebacate).

[14] S.H. Lee, K.-W. Lee, P.S. Gade, A.M. Robertson, Y. Wang, Microwave-assisted facile fabrication of porous poly (glycerol sebacate) scaffolds, Journal of biomaterials science. Polymer edition 29 (2018) 907–916.

[15] Divya Sivanesan, Rama S. Verma, Edamana Prasad, 5FU encapsulated polyglycerol sebacate nanoparticles as anti-cancer drug carriers, RSC Advances 11 (2021) 18984–18993.

[16] Y. Li, W. Huang, W.D. Cook, Q. Chen, A comparative study on poly(xylitol sebacate) and poly(glycerol sebacate): mechanical properties, biodegradation and cytocompatibility, Biomedical materials (Bristol, England) 8 (2013) 35006.

[17] M.J. Kim, M.Y. Hwang, J. Kim, D.J. Chung, Biodegradable and elastomeric poly(glycerol sebacate) as a coating material for nitinol bare stent, BioMed research international 2014 (2014) 956952.

[18] Y. Liu, K. Tian, J. Hao, T. Yang, X. Geng, W. Zhang, Biomimetic poly(glycerol sebacate)/polycaprolactone blend scaffolds for cartilage tissue engineering, Journal of materials science. Materials in medicine 30 (2019).

[19] P. Piszko, B. Kryszak, A. Piszko, K. Szustakiewicz, Brief review on poly(glycerol sebacate) as an emerging polyester in biomedical application: Structure, properties and modifications, Polimery w medycynie 51 (2021) 43–50.

[20] C.C. Lau, M. Al Qaysi, N. Owji, M.K. Bayazit, J. Xie, J.C. Knowles et al., Advanced biocomposites of poly(glycerol sebacate) and β-tricalcium phosphate by in situ microwave synthesis for bioapplication, Materials Today Advances 5 (2020) 100023.

[21] J.M. Kemppainen, S.J. Hollister, Tailoring the mechanical properties of 3D-designed poly(glycerol sebacate) scaffolds for cartilage applications, Journal of biomedical materials research. Part A 94 (2010) 9–18.

[22] Q.-Z. Chen, A. Bismarck, U. Hansen, S. Junaid, M.Q. Tran, S.E. Harding et al., Characterisation of a soft elastomer poly(glycerol sebacate) designed to match the mechanical properties of myocardial tissue, Biomaterials 29 (2008) 47–57.

[23] Q.-Z. Chen, A. Bismarck, U. Hansen, S. Junaid, M.Q. Tran, S.E. Harding et al., Characterisation of a soft elastomer poly(glycerol sebacate) designed to match the mechanical properties of myocardial tissue, Biomaterials 29 (2008) 47–57.

[24] I. Pomerantseva, N. Krebs, A. Hart, C.M. Neville, A.Y. Huang, C.A. Sundback, Degradation behavior of poly(glycerol sebacate), Journal of biomedical materials research. Part A 91 (2009) 1038–1047.

[25] I.H. Jaafar, M.M. Ammar, S.S. Jedlicka, R.A. Pearson, J.P. Coulter, Spectroscopic evaluation, thermal, and thermomechanical characterization of poly(glycerol-sebacate) with variations in curing temperatures and durations, J Mater Sci 45 (2010) 2525–2529.

[26] P. Denis, M. Wrzecionek, A. Gadomska-Gajadhur, P. Sajkiewicz, Poly(Glycerol Sebacate)-Poly(l-Lactide) Nonwovens. Towards Attractive Electrospun Material for Tissue Engineering, Polymers 11 (2019).

[27] A. Gadomska-Gajadhur, M. Wrzecionek, G. Matyszczak, P. Piętowski, M. Więcław, P. Ruśkowski, Optimization of Poly(glycerol sebacate) Synthesis for Biomedical Purposes with the Design of Experiments, Org. Process Res. Dev. 22 (2018) 1793–1800.

[28] In vivo degradation characteristics of poly(glycerol sebacate).

[29] Y. Jia, W. Wang, X. Zhou, W. Nie, L. Chen, C. He, Synthesis and characterization of poly(glycerol sebacate)-based elastomeric copolyesters for tissue engineering applications, Polym. Chem. 7 (2016) 2553–2564.

[30] R. Rai, M. Tallawi, A. Grigore, A.R. Boccaccini, Synthesis, properties and biomedical applications of poly(glycerol sebacate) (PGS): A review, Progress in Polymer Science 37 (2012) 1051–1078.

[31] J. Gao, P.M. Crapo, Y. Wang, Macroporous elastomeric scaffolds with extensive micropores for soft tissue engineering, Tissue engineering 12 (2006) 917–925.

[32] K.-W. Lee, P.S. Gade, L. Dong, Z. Zhang, A.M. Aral, J. Gao et al., A biodegradable synthetic graft for small arteries matches the performance of autologous vein in rat carotid arteries, Biomaterials 181 (2018) 67–80.

[33] M. Frydrych, B. Chen, Fabrication, structure and properties of three-dimensional biodegradable poly(glycerol sebacate urethane) scaffolds, Polymer 122 (2017) 159–168.

[34] B. Kong, S. Mi, Electrospun Scaffolds for Corneal Tissue Engineering: A Review, Materials (Basel, Switzerland) 9 (2016).

[35] R. Sridhar, S. Sundarrajan, J.R. Venugopal, R. Ravichandran, S. Ramakrishna, Electrospun inorganic and polymer composite nanofibers for biomedical applications, Journal of biomaterials science. Polymer edition 24 (2013) 365–385.

[36] I. Jun, H.-S. Han, J.R. Edwards, H. Jeon, Electrospun Fibrous Scaffolds for Tissue Engineering: Viewpoints on Architecture and Fabrication, International journal of molecular sciences 19 (2018).

[37] D.G.T. Strange, K. Tonsomboon, M.L. Oyen, Electrospun Fiber - Hydrogel Composites for Nucleus Pulposus Tissue Engineering, MRS Proc. 1417 (2012).

[38] K. Asadi-Pakdel, R. Mehdinavaz Aghdam, M. Shahedi Asl, M.A. Faghihi Sani, Synthesis and morphology optimization of electrospun SiBNC nanofibers, Ceramics International 46 (2020) 6052–6059.

[39] E.M. Jeffries, R.A. Allen, J. Gao, M. Pesce, Y. Wang, Highly elastic and suturable electrospun poly(glycerol sebacate) fibrous scaffolds, Acta biomaterialia 18 (2015) 30–39.

[40] F. Flaig, H. Ragot, A. Simon, G. Revet, M. Kitsara, L. Kitasato et al., Design of Functional Electrospun Scaffolds Based on Poly(glycerol sebacate) Elastomer and Poly(lactic acid) for Cardiac Tissue Engineering, ACS biomaterials science & engineering 6 (2020) 2388–2400.

[41] M. Biggs, A. Pandit, D.I. Zeugolis, 2D imprinted substrates and 3D electrospun scaffolds revolutionize biomedicine, Nanomedicine (London, England) 11 (2016) 989–992.

[42] Y. Li, G.A. Thouas, Q.-Z. Chen, Biodegradable soft elastomers: synthesis/properties of materials and fabrication of scaffolds, RSC Adv. 2 (2012) 8229.

[43] L. Vogt, F. Ruther, S. Salehi, A.R. Boccaccini, Poly(Glycerol Sebacate) in Biomedical Applications-A Review of the Recent Literature, Advanced healthcare materials 10 (2021) e2002026.

[44] B. Liang, Q. Shi, J. Xu, Y.-M. Chai, J.-G. Xu, Poly (Glycerol Sebacate)-Based Bio-Artificial Multiporous Matrix for Bone Regeneration, Front. Chem. 0 (001) 1097.

[45] B. Kong, W. Sun, G. Chen, S. Tang, M. Li, Z. Shao et al., Tissue-engineered cornea constructed with compressed collagen and laser-perforated electrospun mat, Scientific reports 7 (2017) 970.

[46] T. Li, Y. Liang, Z. Wang, W. Zhang, L. Wang, Q. Zhou et al., Tissue-engineered scaffold based on carboxymethyl chitin or chitosan for corneal epithelial transplantation, Polym J 50 (2018) 511–521.

[47] N. Zanjanizadeh Ezazi, R. Ajdary, A. Correia, E. Mäkilä, J. Salonen, M. Kemell et al., Fabrication and Characterization of Drug-Loaded Conductive Poly(glycerol sebacate)/Nanoparticle-Based Composite Patch for Myocardial Infarction Applications, ACS Applied Materials & Interfaces 12 (2020) 6899–6909.

[48] K.L. Christman, R.J. Lee, Biomaterials for the treatment of myocardial infarction, Journal of the American College of Cardiology 48 (2006) 907–913.

[49] E.R. Aurand, J. Wagner, C. Lanning, K.B. Bjugstad, Building biocompatible hydrogels for tissue engineering of the brain and spinal cord, Journal of functional biomaterials 3 (2012) 839–863.

[50] X. Gu, F. Ding, Y. Yang, J. Liu, Construction of tissue engineered nerve grafts and their application in peripheral nerve regeneration, Progress in neurobiology 93 (2011) 204–230.

[51] U. Till, L. Gibot, A.-F. Mingotaud, J. Ehrhart, L. Wasungu, C. Mingotaud et al., Drug Release by Direct Jump from Poly(ethylene-glycol-b-ε-caprolactone) Nano-Vector to Cell Membrane, Molecules (Basel, Switzerland) 21 (2016).

[52] C.A. Sundback, J.Y. Shyu, Y. Wang, W.C. Faquin, R.S. Langer, J.P. Vacanti et al., Biocompatibility analysis of poly(glycerol sebacate) as a nerve guide material, Biomaterials 26 (2005) 5454–5464.

[53] Matthew Trese, Caio V. Regatieri, Michael J. Young, Advances in Retinal Tissue Engineering.

[54] L.F. Marcos, S.L. Wilson, P. Roach, Tissue engineering of the retina: from organoids to microfluidic chips, Journal of tissue engineering 12 (2021) 20417314211059876.

[55] J.S. Mehta, V. Kocaba, G.S. Peh, A prognostic biomarker of corneal repair, Nature biomedical engineering 3 (2019) 945–946.

[56] C.D. Pritchard, K.M. Arnér, R.A. Neal, W.L. Neeley, P. Bojo, E. Bachelder et al., The use of surface modified poly(glycerol-co-sebacic acid) in retinal transplantation, Biomaterials 31 (2010) 2153–2162.

[57] C.D. Pritchard, K.M. Arnér, R.S. Langer, F.K. Ghosh, Retinal transplantation using surface modified poly(glycerol-co-sebacic acid) membranes, Biomaterials 31 (2010) 7978–7984.

[58] S. Salehi, T. Bahners, J.S. Gutmann, S.-L. Gao, E. Mäder, T.A. Fuchsluger, Characterization of structural, mechanical and nano-mechanical properties of electrospun PGS/PCL fibers, RSC Adv 4 (2014) 16951–16957.

[59] B. Yang, W. Lv, Y. Deng (Eds.), Drug loaded poly(glycerol sebacate) as a local drug delivery system for the treatment of periodontal disease, 2017.

[60] Z.J. Sun, C. Chen, M.Z. Sun, C.H. Ai, X.L. Lu, Y.F. Zheng et al., The application of poly (glycerol-sebacate) as biodegradable drug carrier, Biomaterials 30 (2009).

[61] A. Zamboulis, E.A. Nakiou, E. Christodoulou, D.N. Bikiaris, E. Kontonasaki, L. Liverani et al., Polyglycerol Hyperbranched Polyesters: Synthesis, Properties and Pharmaceutical and Biomedical Applications, International journal of molecular sciences 20 (2019).

[62] M.L. Muerza-Cascante, D. Haylock, D.W. Hutmacher, P.D. Dalton, Melt electrospinning and its technologization in tissue engineering, Tissue engineering. Part B, Reviews 21 (2015) 187–202.

[63] S.S. Rane, P. Choi, Polydispersity Index: How Accurately Does It Measure the Breadth of the Molecular Weight Distribution?, Chemistry of Materials 17 (2005) 926.

[64] M. Li, W. Xu, Y. Su, Solid-state NMR spectroscopy in pharmaceutical sciences, TrAC Trends in Analytical Chemistry 135 (2021) 116152.

[65] J.D. Mallet, P.J. Rochette, Wavelength-dependent ultraviolet induction of cyclobutane pyrimidine dimers in the human cornea, Photochemical & photobiological sciences Official

journal of the European Photochemistry Association and the European Society for Photobiology 12 (2013) 1310–1318.

[66] M.S.H. Akash, Essentials of Pharmaceutical Analysis, Springer Singapore Pte. Limited, Singapore, 2020.

[67] The Conservation of Orbital Symmetry, Elsevier, 1971.

[68] F.A. Carey, Organic chemistry, 4th ed., McGraw-Hill, Boston, 2000.

[69] E.R. Alfenas, J.G.B.P.C.P. da Silva, M.E.S. Silveira, M.F.L. Fonseca, J.A.A. de Arruda, A. Moreno, A Painting Technique Using Ceramic Pigments for the Artificial Iris of an Ocular Prosthesis Guided by Applying Newton's Color Wheel, Journal of prosthodontics official journal of the American College of Prosthodontists 28 (2019) e822-e825.

[70] X. Lei, Y.-G. Jia, W. Song, D. Qi, J. Jin, J. Liu et al., Mechanical and Optical Properties of Reinforced Collagen Membranes for Corneal Regeneration through Polyrotaxane Cross-Linking, ACS Applied Bio Materials 2 (2019) 3861–3869.

[71] P. van der Heide, X-ray photoelectron spectroscopy: An introduction to principles and practices, Wiley, Hoboken N.J., 2012.

[72] M.P. Krompiec, S.N. Baxter, E.L. Klimareva, D.S. Yufit, D.G. Congrave, T.K. Britten et al., 3,4-Phenylenedioxythiophenes (PheDOTs) functionalized with electron-withdrawing groups and their analogs for organic electronics, J. Mater. Chem. C 6 (2018) 3743–3756.